

UC Santa Cruz

UC Santa Cruz Previously Published Works

Title

Siderophile element constraints on the thermal history of the H chondrite parent body.

Permalink

<https://escholarship.org/uc/item/16c210vw>

Authors

Archer, Gregory J

Walker, Richard J

Tino, Jonathan

et al.

Publication Date

2019

DOI

10.1016/j.gca.2018.11.012

Peer reviewed



Siderophile element constraints on the thermal history of the H chondrite parent body

Gregory J. Archer^{a,b,*}, Richard J. Walker^a, Jonathan Tino^a, Terrence Blackburn^c
Thomas S. Kruijer^{b,d}, Jan L. Hellmann^b

^a Department of Geology, University of Maryland, College Park, MD 20742, USA

^b Institut für Planetologie, University of Münster, Münster 48149, Germany

^c Earth and Planetary Sciences, University of California, Santa Cruz, Santa Cruz, CA 95064, USA

^d Nuclear and Chemical Sciences Division, Lawrence Livermore National Laboratory, Livermore, CA 94550, USA

Received 23 March 2018; accepted in revised form 9 November 2018; available online 20 November 2018

Abstract

The abundances of highly siderophile elements (HSE: Re, Os, Ir, Ru, Pt, Pd), as well as ^{187}Re - ^{187}Os and ^{182}Hf - ^{182}W isotopic systematics were determined for separated metal, slightly magnetic, and nonmagnetic fractions from seven H4 to H6 ordinary chondrites. The HSE are too abundant in nonmagnetic fractions to reflect metal-silicate equilibration. The disequilibrium was likely a primary feature, as ^{187}Re - ^{187}Os data indicate only minor open-system behavior of the HSE in the slightly and non-magnetic fractions. ^{182}Hf - ^{182}W data for slightly magnetic and nonmagnetic fractions define precise isochrons for most meteorites that range from 5.2 ± 1.6 Ma to 15.2 ± 1.0 Ma after calcium aluminum inclusion (CAI) formation. By contrast, ^{182}W model ages for the metal fractions are typically 2–5 Ma older than the slope-derived isochron ages for their respective, slightly magnetic and nonmagnetic fractions, with model ages ranging from 1.4 ± 0.8 Ma to 12.6 ± 0.9 Ma after CAI formation. This indicates that the W present in the silicates and oxides was not fully equilibrated with the metal when diffusive transport among components ceased, consistent with the HSE data. Further, the W isotopic compositions of size-sorted metal fractions from some of the H chondrites also differ, indicating disequilibrium among some metal grains. The chemical/isotopic disequilibrium of siderophile elements among H chondrite components is likely the result of inefficient diffusion of siderophile elements from silicates and oxides to some metal and/or localized equilibration as H chondrites cooled towards their respective Hf-W closure temperatures. The tendency of ^{182}Hf - ^{182}W isochron ages to young from H5 to H6 chondrites may indicate derivation of these meteorites from a slowly cooled, undisturbed, concentrically-zoned parent body, consistent with models that have been commonly invoked for H chondrites. Overlap of isochron ages for H4 and H5 chondrites, by contrast, appear to be more consistent with shallow impact disruption models.

The W isotopic composition of metal from one CR chondrite was examined to compare with H chondrite metals. In contrast to the H chondrites, the CR chondrite metal is characterized by an enrichment in ^{183}W that is consistent with nucleosynthetic *s*-process depletion. Once corrected for the correlative nucleosynthetic effect on ^{182}W , the ^{182}W model age for this meteorite of 7.0 ± 3.6 Ma is within the range of model ages of most metal fractions from H chondrites. The metal is therefore too young to be a direct nebular condensate, as proposed by some prior studies.

© 2018 Elsevier Ltd. All rights reserved.

Keywords: H chondrites; Thermochronology; Onion shell; Highly siderophile elements; Os isotopes; W isotopes; CR chondrites; Nucleosynthetic

* Corresponding author at: Institut für Planetologie, University of Münster, Münster 48149, Germany.

E-mail address: archer@uni-muenster.de (G.J. Archer).

1. INTRODUCTION

Chondrites are unmelted aggregates of primitive components that formed in different early Solar System environments. Consequently, the components of which they are comprised were initially in chemical and isotopic disequilibrium. These components can include refractory inclusions (e.g., calcium-aluminum-rich inclusions; CAI), chondrules, matrix, and Fe, Ni metal. The H chondrites experienced a wide range of thermal-metamorphic conditions, ranging from petrologic type H3, with peak temperatures of 400–600 °C, through petrologic types H4 to H6, with peak temperatures ranging from 500 to 1000 °C (e.g., Keil, 2000; Slater-Reynolds and McSween, 2005). Comparison of H4 through H6 chondrites has shown increasing degrees of chemical equilibration of some elements (e.g., Fe and Mg in olivine) and textural integration of chondritic components, such as a decrease in the abundance of identifiable chondrules, with increasing petrologic type (e.g., Rubin, 2000; Rubin et al., 2001; Huss et al., 2006; Weisberg et al., 2006).

Some prior studies have proposed an onion-shell thermal model for the parent body of H chondrites to explain correlations between H chondrite petrologic type and closure ages for multiple temperature-sensitive systems, including fission tracks (Pellas and Storzer, 1981; Trieloff et al., 2003), and ^{207}Pb - ^{206}Pb (e.g., Göpel et al., 1994). In this model, the parent body is assumed to be internally heated by the decay of now-extinct ^{26}Al ($t_{1/2} = 0.7$ Ma; Norris et al., 1983). Those H chondrites that were located deepest within the parent body reached the highest temperatures, cooled slowest, and therefore, experienced the highest degrees of thermal metamorphism. By contrast, those chondrites that were closer to the surface cooled more rapidly and experienced lower degrees of thermal metamorphism. Thus, according to this model, H chondrites of higher petrologic type, which were deeper in the parent body, should record the youngest closure ages for each radiogenic isotope system.

The short-lived ^{182}Hf - ^{182}W radiogenic isotopic system ($t_{1/2} = 8.9$ Ma; Vockenhuber et al., 2004) is useful for constraining processes that occurred during the first ~50 million years of Solar System history. It is especially useful for constraining the timing of metal-silicate equilibration, because W is moderately siderophile and strongly partitions into metals, whereas Hf is lithophile and is retained exclusively in silicates. The system has been widely used to constrain the timing of core formation on planetary bodies (e.g., Lee and Halliday, 1995; Harper and Jacobsen, 1996; Kruijer et al., 2014a), and may also be used as a thermochronometer (Kleine et al., 2008).

Kleine et al. (2008) applied the ^{182}Hf - ^{182}W isotopic system to H chondrite metals and silicates in order to constrain the cooling history of H chondrites after metamorphic heating. That study mathematically estimated closure temperatures of 800–875 °C for H4 through H6 chondrites, using the diffusion model of Van Orman et al. (2001), and concluded that the lower petrologic type H chondrites have older closure ages than higher metamorphic grade H chondrites. Further, by combining Hf-W data

with the different closure ages of multiple other isotopic systems (Pb-Pb, Ar-Ar, and ^{244}Pu fission tracks), they calculated cooling rate curves for the H chondrite parent body, and found an inverse correlation between petrologic types and cooling rates. The consistent relations among closure ages, cooling rates, and petrologic types were interpreted as strong evidence in support of an onion-shell thermal model for the H chondrite parent body. Based on previously reported thermochronological data for H chondrites and thermal modeling, Monnereau et al. (2013) determined that the H chondrite parent body accreted 2 Myr after CAI formation, likely over a duration of 0–0.2 Myr, and similarly concluded that the cooling history of the parent body was consistent with the onion-shell model.

Not all thermal models have supported the onion-shell cooling model. Petrologic observations, along with metallographic cooling rates determined from the Ni diffusion profiles in H chondrite metal, have been interpreted to indicate that parent body cooling was disrupted by one or more impacts, and that cooling may instead have occurred in a rubble pile (e.g., Taylor et al., 1987; Scott et al., 2014; Ruzicka et al., 2015). The onion-shell and disrupted parent body models, however, are evidently not mutually exclusive. Blackburn et al. (2017) reported U-Pb age data for H chondrite phosphates and proposed a model that takes into account initially onion-shell cooling and subsequent disruption by impact. In addition, based on thermal modeling using previously reported thermochronological data, Harrison and Grimm (2010) proposed a ‘perturbed onion-shell model,’ in which the parent body was partially, but not completely, disturbed by impacts.

In addition to conflicting evidence supporting different models for the thermal history of the H chondrite parent body, some early Solar System processes may have led to complexities in the interpretation of thermochronological data. Kleine et al. (2008) noted that some metal fractions from the H5 chondrite Richardton have anomalous W isotopic compositions that cannot be readily explained by the decay of ^{182}Hf in a body with an onion-shell thermal structure. They speculated that the anomalous isotopic compositions could reflect an early irradiation of the metal, leading to a modification (lowering) of its ^{182}W isotopic composition. Also, correlated nucleosynthetic ^{182}W and ^{183}W anomalies have subsequently been reported for some bulk meteorites, including carbonaceous chondrites and carbonaceous chondrite-related iron meteorites (Budde et al., 2016; Kruijer et al., 2014b, 2017). Consequently, nucleosynthetic heterogeneity could also conceivably account for the low ^{182}W isotopic composition observed in Richardton metal.

The chemical and isotopic compositions of metal found in some or all H chondrites have been modified by thermal metamorphism, hence, HSE abundances and ^{182}W isotopic compositions of most H chondrite metals likely do not reflect the characteristics of the metals prior to their incorporation in the parent body. Renazzo-like carbonaceous chondrites (CR chondrites) commonly occur as petrologic type 2, and are characterized by reduced silicates, high abundances of Fe, Ni metal, volatile element depletions, and low degrees of thermal metamorphism (Weisberg

et al., 1995; Krot et al., 2002). Metals present in CR chondrites are, therefore, much less likely to have been chemically or isotopically modified subsequent to incorporation in the parent body. Consistent with this, some prior studies have proposed that CR chondrite metal may have formed by condensation directly from nebular gas (Weisberg et al., 1993), while others have concluded that CR chondrite metal formed via re-condensation of chondrule-derived vapor (Connolly et al., 2001), or reduction (Zanda et al., 1994; Connolly et al., 2001). Comparison of the ^{182}Hf - ^{182}W isotopic systematics of CR chondrite metal with H chondrite metal could, therefore, provide new insights to the timing and nature of chondrite metal formation.

In this study, the ^{182}Hf - ^{182}W systematics of H chondrite metals and oxide-silicate mixtures from seven H chondrites are determined using new analytical techniques that achieve higher precision than prior studies. We also examine the corresponding highly siderophile element (HSE: Re, Os, Ir, Ru, Pt, Pd) abundances and ^{187}Re - ^{187}Os isotopic systematics of the H chondrite components. The concentration data allow an assessment of the degree of siderophile element equilibration between metal and non-metal components (e.g., Horan et al., 2009). The Re-Os isotopic systematics of these components allow an assessment of whether or not siderophile element distributions among components have been disturbed by impact or other processes subsequent to the first few 10s of Ma of Solar System history. We also determine the ^{182}W composition of the CR2 chondrite Acfer 395 for comparison to H chondrite metals.

The primary goals of this study are to: (1) re-examine the thermal history of the H chondrite parent body using refined Hf-W measurement techniques, (2) explore diffusive exchange of siderophile elements between metals and non-metallic phases in chondrites during thermal metamorphism, (3) investigate whether processes other than ^{182}Hf decay have led to ^{182}W isotopic variability among some H chondrite metal fractions, and (4) compare the timing and formation mechanisms of H chondrite metal to CR chondrite metal.

2. SAMPLES

Seven H chondrites and one CR chondrite were investigated. The H chondrites range from petrologic type 4 to 6, and the CR chondrite is petrologic type 2. The H5 chondrite Faucett (UCLA 416) and the CR2 chondrite Acfer 395 (UCLA 2701) were provided by the University of California Los Angeles Meteorite Collection. The H5 chondrite Richardton was provided by the Carnegie Institution for Science (CIS). All other samples were provided by the Smithsonian Institution National Museum of Natural History (SI), including the H4 chondrite Avanhandava (USNM 6882), H5 chondrites Allegan (USNM 215) and Forest City (USNM 2774 2), and H6 chondrites Oakley (USNM 3350) and ALHA 78115 (USNM 7318 78115,1). Avanhandava, Richardton, Forest City, and Allegan were observed falls, and the other chondrites are finds.

Avanhandava, Richardton, and Allegan were chosen for this study because thermochronological data have previ-

ously been reported for them (e.g., Kleine et al., 2008; Trierloff et al., 2003; Blackburn et al., 2017), allowing comparisons to results from previous studies. Further, Kleine et al. (2008) reported that Richardton metal fractions have anomalous ^{182}W isotopic compositions, highlighting the need for further study. Faucett, Forest City, Oakley, and ALHA 78115 were chosen in order to expand the current subset of H chondrites for which there are thermochronological data, as most studies have exclusively relied on a limited suite of nine samples to assess the thermal structure of the H chondrite parent body.

3. METHODS

3.1. ^{182}Hf - ^{182}W systematics of H chondrites

Components of all samples were separated based on magnetic susceptibility at the University of Maryland *Isotope Geochemistry Laboratory (IGL)*. The W isotopic compositions, and Hf and W abundances of metal fractions were determined at the *IGL*. For slightly magnetic and non-magnetic fractions, the W isotopic compositions, and Hf and W abundances were determined at the University of Münster, Institut für Planetologie.

3.1.1. Sample preparation

All samples from the SI and the CIS were previously processed as part of a complementary study on ^{207}Pb - ^{206}Pb dating of separated phosphates from H chondrites (Blackburn et al., 2017). Before being transferred to the University of Maryland for this study, the chondrites from that study were gently crushed using an agate mortar and pestle and then separated by magnetic susceptibility using an *S.G. Frantz*[®] magnetic separator. Detailed methods are provided in Blackburn et al. (2017). Two samples (Faucett and Acfer 395) were processed from bulk chondritic fragments at the *IGL*. They were gently crushed using an agate mortar and pestle, and then a hand magnet was used to separate material into highly magnetic (primarily metal), slightly magnetic (NM-2), and nonmagnetic (NM-1) fractions. Nonmagnetic and slightly magnetic fractions that were separated in different sessions are denoted by A and B suffixes.

Fractions from all samples were purified by repeated crushing using a mortar and pestle while immersed in ultrapure H_2O from a *MilliQ*[®] water purification system, followed by further magnetic separation using a hand magnet. This process was repeated until no further separation of metal from silicate was possible. A hand magnet was used to check that all magnetic material was removed from the nonmagnetic (NM1) fraction. Most adhering nonmagnetic dust was removed from metal fractions by cleaning in an ultrasonic bath, however small fractions of nonmagnetic dust could not be removed. Metal grains were separated into $>150\ \mu\text{m}$ and $<150\ \mu\text{m}$ fractions using a nylon sieve. Conceivably, the $>150\ \mu\text{m}$ and $<150\ \mu\text{m}$ fractions could contain variable portions of fine- and coarse-grained metal, respectively, if coarse metal grains were broken into grains smaller than $150\ \mu\text{m}$, or if fine metal grains were combined together during repeated crushing of fractions.

3.1.2. Separation and purification of W for isotopic compositions

Metal fractions were combined with ~40 mL of 8 M HCl in closed 60 mL Teflon vials and heated to 130 °C for 48 h. The 8 M HCl efficiently digested metal but not silicate, so any W from adhering, Hf-rich silicate phases was dominantly retained in the residue. After digestion of the metals, sample solutions were centrifuged, and the remaining, undigested nonmagnetic phases were separated. A ~0.5% aliquot by volume was then removed, weighed, and spiked with ^{178}Hf and ^{182}W . The remaining sample solution was auto-oxidized in an open beaker by exposure to atmosphere for at least one week, in order to convert Fe^{2+} to Fe^{3+} , so that the Fe^{3+} could be efficiently removed by solvent extraction into diisopropyl ether (Myers and Metzler, 1950). Tungsten was separated and purified using the cation and anion exchange chromatography method reported by Touboul and Walker (2012). After separation and purification of W, all fractions were dried down with either concentrated Teflon-distilled HNO_3 + quartz-distilled HCl, or with Teflon-distilled HNO_3 + H_2O_2 (30%) several times to destroy organics. Total analytical blanks for W were ~1 ng, and blank corrections were insignificant.

Slightly magnetic and nonmagnetic separates were combined with ~15 mL 2:1 concentrated, Teflon-distilled HF- HNO_3 and heated to 120 °C for ~30 h. After digestion, samples were dried and then re-dissolved in concentrated HNO_3 to remove organics. The samples were then completely re-dissolved in 6 M HCl-0.06 M HF, and a 10% aliquot was removed, precisely weighed, and spiked with a mixed ^{180}Hf - ^{183}W spike.

Tungsten was separated and purified using a modified version of the two-stage anion exchange chromatography method reported by prior studies (e.g., Kleine et al., 2004, 2012; Kruijer et al., 2012, 2015). For the first column stage, samples were dissolved in 75 mL 0.5 M HCl-0.5 M HF and then loaded onto pre-cleaned anion exchange columns (4 mL *BioRad* AG1 \times 8, 200–400 mesh). After rinsing the sample matrix with 10 mL 0.5 M HCl-0.5 M HF, W (along with high field strength elements) was eluted with 15 mL 6 M HCl-1 M HF. The samples were dried, and then repeatedly re-dissolved in a few drops each of HNO_3 and H_2O_2 (30%), and dried at 80 °C to remove organics. High field strength elements were removed using a second anion exchange column and the method reported by Kruijer et al. (2015). Samples were further purified of organics using HNO_3 and H_2O_2 . Total procedural blanks for W ranged from 29 to 123 pg, with a mean of 71 pg ($n = 7$). For comparison, the W blanks of Kleine et al. (2008) ranged from ~50–350 pg. Blank corrections were less than 1.5% for most fractions, except for Oakley NM1, which had a blank correction of 7%. A 50% uncertainty for blank corrections is included in each of the reported uncertainties for isotopic compositions.

3.1.3. Mass spectrometry for W isotopic compositions

Purified W from each metal fraction was loaded onto a previously outgassed (48 h before) Re filament using a

method slightly modified from Touboul and Walker (2012). Twenty-four hours after loading W, a mixed activator containing 5 μg each of La and Gd was added (Touboul and Walker, 2012).

The W isotopic compositions of the metal fractions were measured by negative thermal ionization (N-TIMS) on the UMD *Thermo-Fisher Triton 1* using Faraday cup collection. Tungsten was measured as WO_3^- , and oxide production was enhanced by bleeding O_2 ($P_{\text{O}_2} = 1.0 \times 10^{-7}$ mbar) into the source. The N-TIMS method of Touboul and Walker (2012), which allows the measurement of $^{182}\text{W}/^{184}\text{W}$ to a 2SD external precision (defined as the 2SD of solution standards analyzed over the course of 9 months on *Thermo-Fisher Triton 1*) of ~5 ppm, was used for two Faucett metal fractions. For these analyses, $^{183}\text{W}/^{184}\text{W}$ was not measured, as the ratio was assumed to be normal and was used in a second order fractionation correction. A new N-TIMS method, which allowed measurement of both $^{182}\text{W}/^{184}\text{W}$ and $^{183}\text{W}/^{184}\text{W}$ to external precisions of ~5 ppm by measuring in-run O isotopic compositions using $10^{12} \Omega$ resistors on two Faraday cups (H3 and H4), was developed during the course of this study, and was used for all other fractions (Archer et al., 2017). For both N-TIMS methods, instrumental mass bias was corrected using normalizing ratios $^{186}\text{W}/^{184}\text{W} = 0.92767$ and $^{186}\text{W}/^{183}\text{W} = 1.9859$ (Kleine et al., 2004) and the exponential law. Measured signal intensities evolved during analyses, and typically ranged from 0.7 to 1.2 V for ^{184}W .

The W isotopic compositions of slightly magnetic and nonmagnetic separates were measured on the *Thermo-Fisher Neptune Plus* multi collector-inductively coupled plasma mass spectrometer (MC-ICPMS) in the *Institut für Planetologie* at the University of Münster, with an instrumental configuration similar to that used by Kruijer et al. (2014a) and Kruijer et al. (2015), using Faraday cup collection. Samples were introduced using an *ESI* self-aspirating nebulizer and a *Cetac Aridus II* desolvating nebulizer system. A *Jet* sampler and an *X-skimmer cone* were used for optimal sensitivity (intensity of ~1.5– 2×10^{-11} A for 30 ng/g W *Alfa Aesar* laboratory standard). Each measurement consisted of 100–200 cycles, with integration times of 4.2 s. Instrumental mass bias corrections were made using $^{186}\text{W}/^{184}\text{W} = 0.92767$ and $^{186}\text{W}/^{183}\text{W} = 1.9859$ (Kleine et al., 2004) using the exponential law. Signal intensities varied from 0.44 to 11 V for ^{184}W among analyses, depending on the abundance of W in the analyte.

Since the protocol used to measure the W isotopic composition of metals differed from the protocol used to measure nonmagnetic and slightly magnetic fractions, it is critical that these two protocols produce comparable results. Archer et al. (2017) compared the results of samples measured using the two procedures detailed above, and reported that the ^{182}W and ^{183}W isotopic compositions were identical within uncertainties. Mundl et al. (2018) also compared data for *NIST* steel standard 129c processed using these two procedures, and found that the ^{182}W and ^{183}W isotopic compositions were also in agreement within uncertainties.

3.1.4. Hafnium and W concentrations by isotope dilution

Spiked-sample mixtures from metal fractions were equilibrated in closed 15 mL vials on a hotplate at 120 °C for 24 h. After drying, spike-sample mixtures were re-dissolved in 2 mL of 0.5 M HCl-0.5 M HF. Hafnium and W were then separated and purified using a single-stage anion exchange chromatographic technique (Touboul et al., 2007; Touboul et al., 2009). Purified W and Hf from metal fractions were measured on the UMD *Nu Plasma* MC-ICPMS using Faraday cup collection. Tungsten and Hf standards were analyzed during each analytical session to correct for instrumental bias. Blanks for W ranged from 10 pg to 84 pg, with a mean of 51 pg (n = 4). Hafnium blanks ranged from 15 pg to 122 pg, with a mean of 47 pg (n = 4). Because metal fractions have low Hf concentrations, Hf blank corrections exceeded 50% for some samples. Uncertainties for blank corrections are reflected in the reported uncertainties for $^{180}\text{Hf}/^{184}\text{W}$.

Unlike metal fractions, the $^{180}\text{Hf}/^{182}\text{W}$ of slightly magnetic and nonmagnetic fractions were highly variable, and precise determinations of $^{180}\text{Hf}/^{184}\text{W}$ were critical. Therefore, care was taken to increase the abundance ratio of sample to blank. Larger (~10% by volume) aliquots were removed and spiked with appropriate amounts of a mixed ^{180}Hf - ^{183}W tracer. The sample-spike mixtures were equilibrated on a hotplate in closed 15 mL vials at 120 °C overnight. Hafnium and W were separated and purified using a modified version of the method described in Kleine et al., (2004). In order to remove organics, samples were dried and then re-dissolved in several drops of HNO_3 and H_2O_2 . They were then re-dried at 80 °C. After re-dissolving in loading acid (0.56 M HNO_3 -0.24 M HF), spiked Hf and W from slightly magnetic and nonmagnetic fractions were measured on the *Thermo-Fisher Neptune Plus* using Faraday cup collection. Mass bias corrections were made using $^{179}\text{Hf}/^{177}\text{Hf} = 0.7325$ and $^{186}\text{W}/^{184}\text{W} = 0.92768$. Blanks for W ranged from 1 pg to 20 pg, with a mean of 8 pg (n = 3). Blanks for Hf ranged from 5 pg to 24 pg, with a mean of 11 pg (n = 3). Blank corrections were <2% for the W abundances of most fractions, except Oakley NM-1 (17.5%) and Oakley NM-2 (3%). Blank corrections were <1% for the Hf abundances of all fractions. A 50% uncertainty for blank corrections is included in each of the reported uncertainties for $^{180}\text{Hf}/^{184}\text{W}$.

3.2. ^{187}Re - ^{187}Os isotopic systematics and HSE abundances

Metal fractions (>150 μm and <150 μm) and nonmagnetic (NM1) fractions from Avanhandava (H4), Richardton (H5), and ALHA 78115 (H6) were separately combined with a 2:1 mixture of Teflon distilled, concentrated HNO_3 + HCl, and two isotopic spikes, one enriched in ^{185}Re and ^{190}Os , the other enriched in ^{191}Ir , ^{99}Ru , ^{194}Pt , and ^{105}Pd . Sample-spike mixtures were sealed in 8 mL PyrexTM Carius tubes (Shirey and Walker, 1995) and heated to 260 °C for 72 h. After digestion, Os was removed via solvent extraction using CCl_4 , and back extraction into Teflon distilled concentrated HBr (Cohen and Waters, 1996).

Separated Os was purified by microdistillation from dichromate into concentrated HBr (Birck et al., 1997). Ruthenium, Pd, Re, Ir, and Pt were separated and purified using an anion exchange chromatography technique (Rehkämper and Halliday, 1997). Blank contributions using this method were insignificant, typically comprising <<1% of the total element.

Osmium was measured by N-TIMS on the UMD *Thermo-Fisher Triton 1* using Faraday cup collection. Osmium was loaded onto previously outgassed Pt filaments, and a $\text{Ba}(\text{OH})_2$ activator was added (Creaser et al., 1991). All other HSE were measured as solutions on the UMD *Nu Plasma* MC-ICPMS using Faraday cup collection. The data were corrected for instrumental bias by repeated measurement of a *Johnson Matthey* in-house reference material during each analytical session. Corrections were typically <0.1%.

3.3. High-precision osmium isotopic compositions of H chondrite metal fractions

Metal fractions from Richardton (H5), Allegan (H5), and Oakley (H6) were combined with ~3 mL 8 N HCl in 15 mL Savillex[®] Teflon vials and digested on a hotplate at 130 °C for 48 h. As with the metal fractions measured for W isotopic compositions, a residue of nonmagnetic (silicate and oxide) material remained after digestion, so sample solutions were centrifuged and the nonmagnetic material was removed. Samples and 3 mL of a 2:1 mixture of Teflon distilled, concentrated HNO_3 + HCl were then sealed in 8 mL PyrexTM Carius tubes (Shirey and Walker, 1995) and heated to 260 °C for 24 h. Osmium separation and purification followed the procedures described in Section 3.2. Osmium was measured using a method similar to that described in Section 3.2. Mass bias corrections were made using $^{192}\text{Os}/^{188}\text{Os} = 3.08271$ (Allègre and Luck, 1980), which is optimal for investigating neutron capture reactions (Walker, 2012). Signal intensities ranged from ~1 to ~1.5 V for ^{192}Os during each analysis. External precisions (2SD) for these high-precision measurements were ~±5 ppm.

4. RESULTS

4.1. Highly siderophile element abundances, ^{187}Re - ^{187}Os isotopic compositions, and high precision Os

In order to investigate the diffusive exchange of HSE during thermal metamorphism, a metal fraction and a nonmagnetic (NM1) fraction from one H chondrite of each petrologic type (H4, H5, and H6) was analyzed for HSE abundances and Re-Os isotopic systematics (Table 1; Figs. 1 and 2). The HSE characteristics of metal and nonmagnetic fractions from the 3 H chondrites investigated here are broadly similar to those previously reported for an H3.8 and an H4 chondrite (Horan et al., 2009). Palladium/Os for the Avanhandava (H4) and ALHA 78115 (H6) nonmagnetic fractions are higher than the Pd/Os of Richardton (H5) and the previously reported H3.8 and H4 chondrites. Rhenium/Os varies systematically among the three

Table 1

Highly siderophile element abundances (in ppb) and ^{187}Re - ^{187}Os systematics of H chondrite metal and nonmagnetic (NM1) fragments. Δ_{Os} is the deviation in parts per 10,000 from a primordial 4568 Ma reference isochron. Uncertainties for $^{187}\text{Re}/^{188}\text{Os}$, $^{187}\text{Os}/^{188}\text{Os}$, and Δ_{Os} are 2σ .

	Mass (g)	Re	Os	Ir	Ru	Pt	Pd	$^{187}\text{Os}/^{188}\text{Os}$	2σ	$^{187}\text{Re}/^{188}\text{Os}$	2σ	Δ_{Os}	2σ
<i>Avanhandava (H4)</i>													
>150 μm metal	0.00761	162.3	1490	1422	2256	3197	2642	0.13654	0.00041	0.5273	0.0009	-3.3	0.7
<150 μm metal	0.01123	302.5	3652	3083	4687	6568	3621	0.12889	0.00022	0.4003	0.0007	21	0.6
NM1	0.16794	5.747	88.92	83.03	125.8	70.74	57.61	0.12446	0.00012	0.3121	0.0009	46	0.7
<i>Richardton (H5)</i>													
>150 μm metal	0.00575	190.2	1871	1740	2916	4036	2784	0.13401	0.00029	0.4920	0.0010	-0.6	0.8
<150 μm metal	0.00907	607.9	6663	5785	8492	12,910	6489	0.13091	0.00016	0.4410	0.0009	8.7	0.7
NM1	0.32782	0.504	8.868	10.31	13.72	8.723	2.107	0.11294	0.00012	0.2739	0.0010	-39	0.8
<i>ALHA 78115 (H6)</i>													
>150 μm metal	0.00717	266.2	2743	2464	4003	5803	3118	0.13249	0.00025	0.4696	0.0008	1.8	0.7
<150 μm metal	0.00998	396.7	4626	3761	6214	8701	5250	0.12995	0.00026	0.4144	0.0009	20	0.7
NM1	0.15281	10.02	149.8	146.5	187.8	213.6	86.05	0.12255	0.00007	0.3231	0.0007	18	0.5

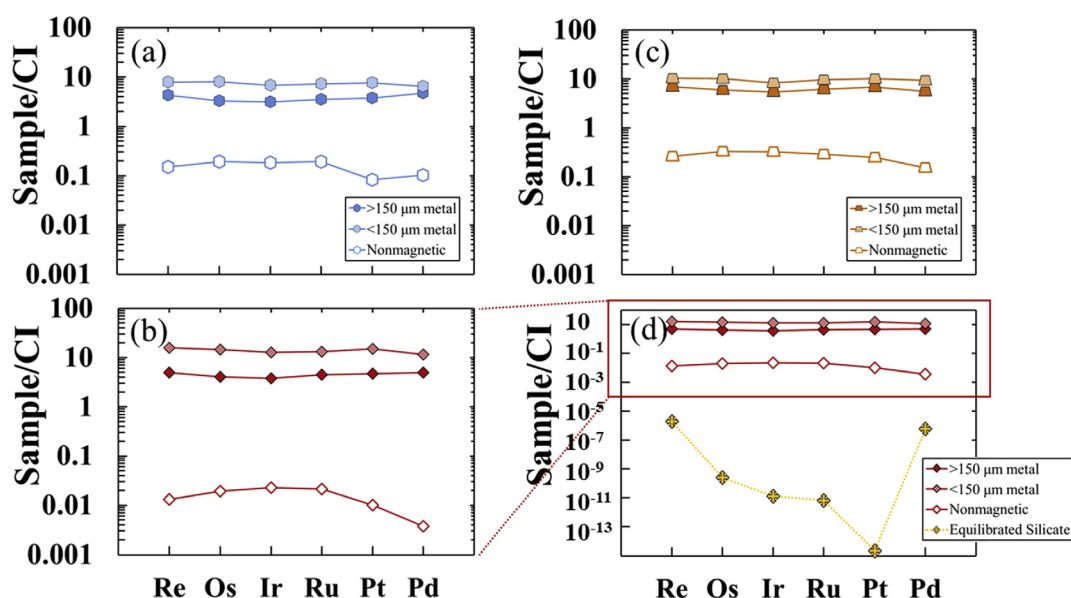


Fig. 1. Orgueil (CI) normalized (CI data from Horan et al., 2003) HSE abundances of: (a) Avanhandava (H4), (b) Richardton (H5), (c) ALHA 78115 (H6) metal and nonmagnetic fractions. Metal fractions are divided into $>150 \mu\text{m}$ and $<150 \mu\text{m}$. (d) calculated composition of nonmagnetic fraction (gold crosses) in equilibrium with Richardton $<150 \mu\text{m}$ metal; Richardton metal and nonmagnetic fractions included for comparison. Metal/silicate D values taken from Walter et al. (2000) and references therein. Uncertainties are smaller than symbol size.

components, with $>150 \mu\text{m}$ metal having the highest ratio, and nonmagnetic fractions having the lowest.

Fine- and coarse-grained metals have supra-chondritic HSE abundances that range from $\sim 3\times$ to $\sim 15\times$ CI for Os, which is similar to the range of previously reported Os abundances for H3.8 and H4 chondrite metal (~ 3 to $\sim 19\times$ CI Os; Horan et al., 2009). The relative abundances of HSE (e.g., Pt/Os) are similar to those of bulk chondrites. For the three H chondrites, fine-grained metal fractions have higher HSE abundances than coarse-grained metal fractions, as was also observed for the H chondrites examined by Horan et al. (2009). The abundances of HSE in the $>150 \mu\text{m}$ metal fractions increase with petrologic type. By contrast, the HSE abundances of the $<150 \mu\text{m}$ metal do not correlate with petrologic type. The $<150 \mu\text{m}$ metal

fraction from Richardton (H5) has the highest HSE abundances, and the $<150 \mu\text{m}$ metal fraction from Avanhandava (H4) has the lowest.

Nonmagnetic fractions have sub-chondritic HSE abundances, ranging from ~ 0.02 – $0.3\times$ CI for Os, which is similar to the range of previously reported Os abundances in nonmagnetic fractions of H3.8 and H4 chondrites (~ 0.04 to $\sim 0.2\times$ CI Os; Horan et al., 2009). Abundances of the HSE are moderately fractionated relative to bulk chondrites, with sub-chondritic Re/Os and Pd/Os that range from 0.057 to 0.067 and 0.24 to 0.65, respectively, compared to ratios averaging 0.084 and 1.2, respectively, for CI chondrites (Horan et al., 2003). Nonmagnetic fractions of Avanhandava and Richardton are also depleted in Pt relative to Os, with Pt/Os of 0.80 and 0.98, respectively,

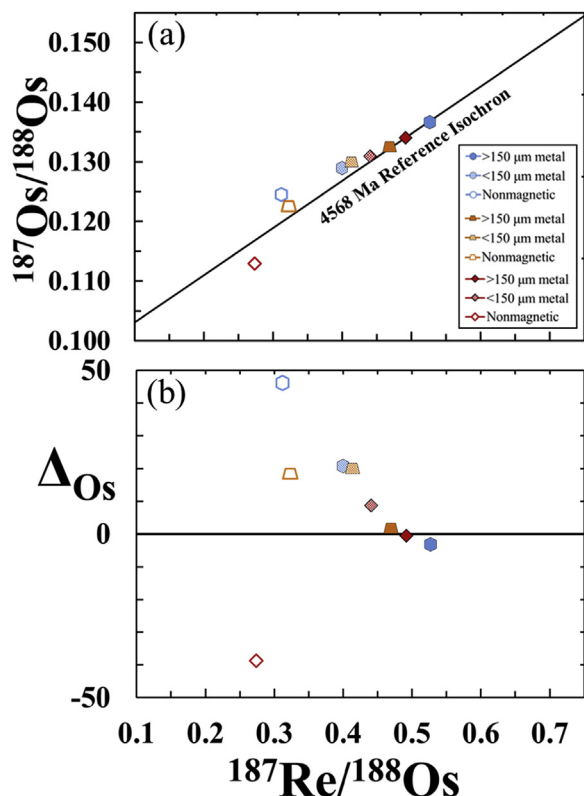


Fig. 2. (a) $^{187}\text{Re}/^{188}\text{Os}$ vs. $^{187}\text{Os}/^{188}\text{Os}$ for H chondrite metal and nonmagnetic fractions from Avanhandava (H4), Richardton (H5), and ALHA 78115 (H6). Symbols are the same as in Fig. 1. A 4568 Ma reference isochron is shown for comparison, using parameters from Archer et al. (2014). Uncertainties are smaller than symbol size. (b) $^{187}\text{Re}-^{187}\text{Os}$ vs. ΔOs , where ΔOs is the deviation in parts per 10,000 from the 4568 Ma reference isochron.

compared to an average CI ratio of 1.9 (Horan et al., 2003). The abundances of HSE in nonmagnetic fractions do not show a systematic relation with petrologic type. The nonmagnetic fraction from Richardton (H5) has the lowest HSE abundances of the three chondrites examined, and the nonmagnetic fraction from ALHA 78115 (H6) has the highest.

The deviation of samples from a primordial 4568 Ma $^{187}\text{Re}-^{187}\text{Os}$ isochron (Fig. 2a), caused by secondary remobilization of Re and/or Os, can be expressed using the ΔOs notation (e.g., Becker et al., 2001; Archer et al., 2014):

$$\Delta\text{Os} = 10^4 \left[\frac{^{187}\text{Os}}{^{188}\text{Os}}_{\text{sample}} - \left(0.09517 + 0.07908 \times \frac{^{187}\text{Re}}{^{188}\text{Os}}_{\text{sample}} \right) \right] \quad (1)$$

where $^{187}\text{Os}/^{188}\text{Os}_{\text{sample}}$ and $^{187}\text{Re}/^{188}\text{Os}_{\text{sample}}$ are the measured $^{187}\text{Os}/^{188}\text{Os}$ and $^{187}\text{Re}/^{188}\text{Os}$ of a sample, and 0.09517 and 0.07908 are the inferred initial $^{187}\text{Os}/^{188}\text{Os}$ of the Solar System, and slope of a 4568 Ma primordial isochron, respectively (Archer et al., 2014), assuming a ^{187}Re decay constant of $1.666 \times 10^{-11} \text{ yr}^{-1}$ (Smoliar et al., 1996). The $^{187}\text{Re}-^{187}\text{Os}$ systematics of coarse-grained metal shows little deviation from a primordial isochron (<3.3

Table 2
 $\mu^{189}\text{Os}$ and $\mu^{190}\text{Os}$ values and 2σ uncertainties of H chondrite metal fractions.

Sample	$\mu^{189}\text{Os}$	2σ	$\mu^{190}\text{Os}$	2σ
Richardton (H5)	-7.2	4.6	0.3	6.4
Allegan (H5)	-1.2	4.6	1.6	6.4
Oakley (H6)	-0.9	4.6	-4.7	6.4

$\mu^x\text{Os}$ is defined as the part per million deviation of the measured isotopic composition of a sample from the Johnson-Matthey internal UMD laboratory standard.

$\pm 0.7 \Delta\text{Os}$ units, Fig. 2b). By contrast, the ΔOs values of fine-grained metal and nonmagnetic fractions deviate by as much as 21 and 46 units, respectively.

The high-precision Os isotopic compositions of 3 H chondrite metal fractions are reported in Table 2, and shown in Fig. 3. The isotopic compositions are reported in $\mu^x\text{Os}$ units, which is the deviation in parts per million of the measured isotopic composition of a sample from the Johnson-Matthey internal UMD reference material. Allegan and Oakley have $\mu^{189}\text{Os}$ and $\mu^{190}\text{Os}$ values that are within uncertainties of the laboratory reference material values. By contrast, Richardton metal has a $\mu^{189}\text{Os}$ value of -7.2 ± 4.6 , which is significantly depleted compared to the reference material.

4.2. Hafnium and W abundances, $^{182}\text{Hf}-^{182}\text{W}$ isotopic compositions, and ^{183}W

Hafnium and W abundances, and the $^{182}\text{Hf}-^{182}\text{W}$ and ^{183}W isotopic compositions of H chondrite metal, slightly magnetic, and nonmagnetic fractions from H4-6 chondrites, and the CR chondrite Acfer 395 are reported in Table 3.

Hafnium abundances for H chondrite metal fractions are typically low, ranging from 2 ppb to 17 ppb for most samples. Forest City $<150 \mu\text{m}$ metal is higher, with 36 ppb Hf. The presence of some Hf in the metal fractions may be the result of silicate inclusions within the metal, as argued by Quitté et al. (2005) for stony-iron meteorites, or because a small amount of Hf was accessed from adhering silicates, which could not be fully removed from the metal fractions (see Section 3.1). The W abundances for the H chondrite metal fractions range from 420 ppb to 960 ppb. The abundances are consistent with prior studies (Rambaldi, 1976; Kong and Ebihara, 1996; Humayun and Campbell, 2002; Kleine et al., 2008). Nonmagnetic and slightly magnetic fractions from most H chondrites (excluding Avanhandava) have W abundances that range from 1.8 ppb to 53.9 ppb. By contrast, nonmagnetic and slightly magnetic fractions from Avanhandava have higher W abundances that range from 108 ppb to 338 ppb. The Hf abundances are similar among all nonmagnetic and slightly magnetic fractions, and considerably higher than those of metal fractions, ranging from 125 ppb to 208 ppb. Collectively, $^{180}\text{Hf}/^{184}\text{W}$ ratios range from 0.003 to 0.091 for metal fractions and 0.578 to 140 for nonmagnetic and slightly magnetic fractions. The fractions with the highest $^{180}\text{Hf}/^{184}\text{W}$ probably contain a large proportion of

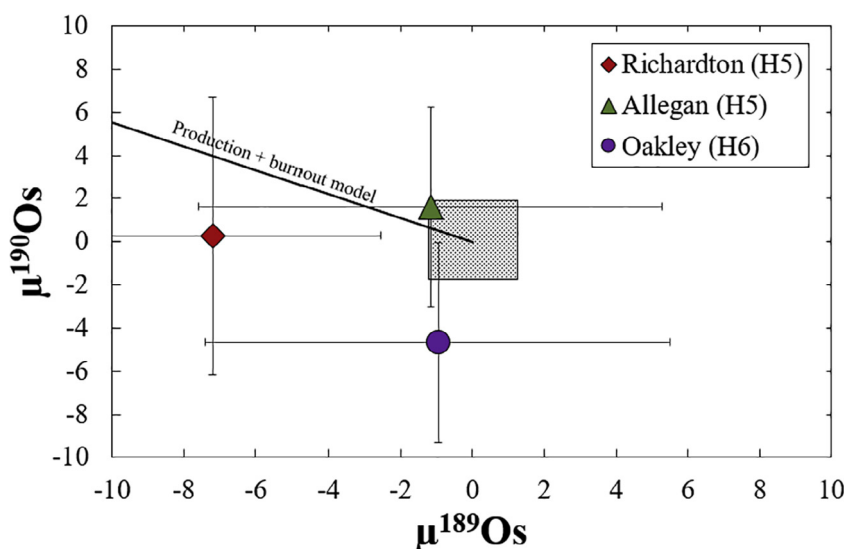


Fig. 3. $\mu^{189}\text{Os}$ vs. $\mu^{190}\text{Os}$ values of H chondrite metal fractions. Production and burnout model line from Walker (2012). Error bars represent 2σ external reproducibility of standard analyses. Grey box represents the 2SE of standard analyses.

high-Ca pyroxene and/or ilmenite, as these are major Hf carriers (Richter and Shearer, 2003).

The relatively high W contents of the nonmagnetic and slightly magnetic fractions, compared to other H chondrites examined here, are consistent with the possibility that the Avanhandava fractions were contaminated with terrestrial W. The low HSE abundances for Avanhandava nonmagnetic fractions, the precise Hf-W isochron for nonmagnetic and slightly magnetic fractions (see Section 5.3), and modelling the effect of terrestrial contamination on the Hf-W systematics of an H chondrite (see electronic annex), however, suggests that terrestrial contamination was unlikely. Thus, the high W abundances of these fractions more likely reflect extreme disequilibrium among metals and silicates/oxides, and represents a primary feature (see electronic annex).

The $\epsilon^{183}\text{W}$ values (defined as the part in 10,000 deviation of $^{183}\text{W}/^{184}\text{W}$ from an in-house W *Alfa Aesar* plasma standard) of H chondrite metal grains measured by TIMS are within the 2SD of the standard. By contrast, some nonmagnetic and slightly magnetic fractions measured by MC-ICP-MS, as well as rock standards BHVO-2 and DTS-2b, which were measured during each session (see Fig. S1 in electronic annex), have resolvably negative $\epsilon^{183}\text{W}$ values, relative to the *Alfa Aesar* laboratory standard. Similar negative ^{183}W values have been reported for various types of samples, including iron meteorites, and silicate-rich samples (e.g., Willbold et al., 2011; Kruijer et al., 2012) measured by MC-ICP-MS. Because terrestrial reference materials measured during this study and previous MC-ICP-MS studies had similar deficits in ^{183}W , but no resolvable deficits in ^{182}W , the negative values most likely reflect analytical artifacts only affecting ^{183}W , rather than the true ^{183}W of the samples. The reason for this analytical artifact is currently not well understood, but could be the result of nuclear field shift effects generated during ion exchange

chromatography, as observed for Nd isotopes (Garçon et al., 2018), or during dry downs and re-dissolutions, as speculated by Willbold et al. (2011) and Cook and Schönbachler (2016). However, the reason these effects are either absent or too small to be observed for the metal fractions measured by TIMS is unclear. Differences in bulk composition (i.e., metal vs. silicate-oxide matrices) of the samples are unlikely to be the cause, as previously reported ^{183}W values for terrestrial, silicate-oxide dominated samples also measured by TIMS appear to be free from these effects (e.g., Mundl et al., 2018). We speculate that it could be due to different column dimensions for the two procedures, or different abundances of W in metals vs. nonmagnetic and slightly magnetic fractions, or the formation of hydrides within the plasma, as proposed by Breton and Quitté (2014). Regardless of the cause, we conclude that the negative $\epsilon^{183}\text{W}$ values for some nonmagnetic and slightly magnetic samples measured by MC-ICP-MS are analytical artifacts, rather than natural ^{183}W variations, whereas the $\epsilon^{183}\text{W}$ values for metal fractions analyzed by TIMS represent their natural ^{183}W isotopic composition.

The $\epsilon^{182}\text{W}$ values (normalized to $^{186}\text{W}/^{184}\text{W}$) of $>150\ \mu\text{m}$ metal fractions are indistinguishable, within uncertainties, for H4 and H5 chondrites, with a mean value of -3.14 ± 0.08 (2SD), except for Richardton. The Richardton (H5) $>150\ \mu\text{m}$ metal fraction has a lower $\epsilon^{182}\text{W}$ value of -3.42 ± 0.09 (2SD). Kleine et al. (2008) reported similar, albeit less precise $\epsilon^{182}\text{W}$ values for Richardton coarse-metal fractions (-3.28 ± 0.35 and -3.57 ± 0.16 for $>150\ \mu\text{m}$ and $>230\ \mu\text{m}$ metal fractions, respectively). The $>150\ \mu\text{m}$ metal fraction from H6 chondrite ALHA 78115 has a significantly higher $\epsilon^{182}\text{W}$ value than $>150\ \mu\text{m}$ metal fractions from H4 or H5 chondrites, with a value of -2.97 ± 0.05 (2SD). For some H chondrites examined here, the $<150\ \mu\text{m}$ metal fractions have higher $\epsilon^{182}\text{W}$ values than their respective $>150\ \mu\text{m}$ fractions. The

Table 3

Hafnium and W abundances (in ppb), $^{180}\text{Hf}/^{184}\text{W}$, $\epsilon^{182}\text{W}$, and $\epsilon^{183}\text{W}$ of H chondrite metal, slightly magnetic (NM2) and nonmagnetic (NM1) fractions. Uncertainties are 2σ .

	Hf	W	$^{180}\text{Hf}/^{184}\text{W}$	\pm	$\epsilon^{182}\text{W}_{6/3}$	\pm	$\epsilon^{182}\text{W}_{6/4}$	\pm	$\epsilon^{183}\text{W}_{6/4}$	\pm
<i>Avanhandava (H4)</i>										
Metal >150 μm	2	834	0.003	0.001	-3.10	0.06	-3.14	0.09	-0.09	0.07
NM-1A	165.3	262.0	0.744	0.004	0.71	0.10	0.50	0.10	-0.32	0.12
NM-2A	165.3	337.5	0.578	0.003	0.55	0.10	0.33	0.10	-0.42	0.12
NM-1B	169.1	332.8	0.599	0.003	0.49	0.10	0.33	0.10	-0.20	0.12
NM-2B	193.7	107.8	2.12	0.01	1.37	0.10	1.26	0.10	-0.15	0.12
<i>Faucett (H5)</i>										
Metal >150 μm	7	782	0.011	0.003	-3.08	0.05	-3.09	0.06	n.d.	n.d.
Metal <150 μm	10	642	0.02	0.02	-3.07	0.05	-3.08	0.05	n.d.	n.d.
<i>Allegan (H5)</i>										
Metal >150 μm	12	960	0.015	0.004	-3.12	0.05	-3.13	0.06	-0.03	0.07
Metal <150 μm	12	608	0.023	0.006	-3.02	0.08	-3.10	0.11	-0.13	0.09
NM-1A	160.9	3.10	61.3	0.4	38.2	1.8	38.4	2.0	0.20	0.79
NM-2A	179.0	25.7	8.22	0.04	3.31	0.24	3.31	0.27	-0.06	0.21
NM-1B	125.0	2.62	56.3	0.4	36.37	0.62	36.37	0.79	0.09	0.57
<i>Richardton (H5)</i>										
Metal >150 μm	9	759	0.013	0.002	-3.37	0.07	-3.42	0.09	-0.04	0.08
Metal <150 μm	17	420	0.05	0.01	-3.11	0.05	-3.12	0.07	-0.02	0.06
NM1	168.4	19.1	10.4	0.1	5.27	0.26	5.28	0.27	-0.03	0.19
NM2	179.1	30.9	6.84	0.07	2.50	0.23	2.49	0.18	-0.05	0.12
<i>Forest City (H5)</i>										
Metal >150 μm	13	594	0.026	0.005	-3.18	0.05	-3.19	0.07	0.01	0.07
Metal <150 μm	36	470	0.091	0.008	-2.78	0.05	-2.75	0.06	0.07	0.04
NM1	164.4	24.1	8.04	0.08	2.82	0.25	2.79	0.26	-0.03	0.12
NM2	186.0	43.4	5.06	0.03	0.98	0.21	0.97	0.19	-0.02	0.12
<i>Oakley (H6)</i>										
Metal <150 μm	4	737	0.007	0.002	-2.81	0.07	-2.86	0.09	-0.08	0.08
Oakley NM1	207.9	1.8	140	20	48.0	2.4	47.5	2.7	-0.6	1.2
Oakley NM2	177.8	11.9	17.6	0.3	5.16	0.34	5.32	0.40	0.24	0.22
Oakley NM1.5	203	3.8	63	3	21.67	0.65	21.76	0.91	-0.10	0.82
<i>ALHA 78115 (H6)</i>										
Metal >150 μm	8	876	0.011	0.004	-2.89	0.05	-2.97	0.07	-0.08	0.06
NM1	140.6	52.8	3.14	0.02	0.67	0.10	0.60	0.10	-0.17	0.12
NM2	136.6	53.9	2.99	0.02	-0.32	0.10	-0.52	0.10	-0.30	0.12
<i>Acfer 395 (CR2)</i>										
Metal (unsorted)	45	581	0.09	0.01	-2.46	0.13	-2.11	0.16	0.57	0.15

n.d. – not determined. $\epsilon^{183}\text{W}_{\text{N}/\text{X}}$ is defined as the part per 10,000 deviation of a measured sample isotopic composition from an *Alfa Aesar* solution standard; subscript denotes normalizing isotopes.

difference is greatest for metal fractions from Forest City (H5), which has $\epsilon^{182}\text{W}$ values of -3.19 ± 0.07 and -2.75 ± 0.06 for the >150 μm and <150 μm metal fractions, respectively. Slightly magnetic and nonmagnetic fractions from H chondrites have highly variable $\epsilon^{182}\text{W}$, ranging from -0.5 to $+47.5$. The nonmagnetic (NM1) fractions from all samples, except Avanhandava, have the most radiogenic $\epsilon^{182}\text{W}$ values, corresponding with the highest $^{180}\text{Hf}/^{184}\text{W}$.

In contrast to the ^{183}W data for H chondrites, the $\epsilon^{183}\text{W}$ of the separated metal fraction from Acfer 395 (CR2) measured by TIMS is substantially positive with a $\epsilon^{183}\text{W}$ value of $+0.57 \pm 0.15$. This $\epsilon^{183}\text{W}$ value is similar to previously reported positive $\epsilon^{183}\text{W}$ values for CR chondrite magnetic separates (Budde et al., 2018). We therefore conclude that

the positive $\epsilon^{183}\text{W}$ value is likely representative of the true value for the metal. The $\epsilon^{182}\text{W}$ value (normalized to $^{186}\text{W}/^{184}\text{W}$) of -2.11 ± 0.16 for the unsorted metal of CR2 chondrite Acfer 395 is higher than the $\epsilon^{182}\text{W}$ values of any metals for the H chondrites examined here.

5. DISCUSSION

5.1. ^{187}Re - ^{187}Os isotopic systematics

Due to the limited spread of Re/Os in chondritic components and the long half-life of ^{187}Re (41.6 Ga), the ^{187}Re - ^{187}Os system is not useful for precisely dating the formation or isotopic equilibration of chondritic components. However, it can be used to assess open vs. closed system

behavior of bulk chondrites and their components since formation (e.g., [Becker et al., 2001](#); [Archer et al., 2014](#); [Walker et al., 2018](#)). The ^{187}Re - ^{187}Os isotopic systematics of the $>150\ \mu\text{m}$ metal fractions are generally consistent with system closure since formation as they plot on or very near a primordial isochron ([Fig. 2](#)). By contrast, the $<150\ \mu\text{m}$ metal and nonmagnetic fractions plot beyond uncertainties of a primordial isochron, deviating by as much as $46\ \Delta_{\text{Os}}$ units. Similar minor disturbances of the ^{187}Re - ^{187}Os system are common for bulk chondrites and their components (e.g., [Becker et al., 2001](#); [Walker et al., 2002](#); [Brandon et al., 2012](#); [Archer et al., 2014](#); [Kadlag and Becker, 2016](#)). The most likely cause for open system behavior is terrestrial alteration, during which relatively mobile Re, and to a lesser extent Os, is redistributed. Rhenium and/or Os disturbance has even been observed for some falls ([Walker et al., 2018](#)). The open system behavior observed here, while substantial for the isotopic systematics of some non-metal fractions, indicates movement of a maximum of only a few percent of Re or Os. For example, if the open system behavior is recent, offsets from the primordial isochron indicate only gain or loss of Re, or loss of Os, of $<1\%$. Consequently, the HSE abundances reported here for metal and nonmagnetic fractions most likely reflect their HSE abundances immediately following cessation of diffusive exchange between metal, silicates, and oxides.

5.2. Siderophile element abundances

Because chondrites are aggregates of materials that formed in different places and at different times, their components were probably not in chemical or isotopic equilibrium immediately following aggregation (e.g., [Humayun and Campbell, 2002](#)). Therefore, diffusive exchange of elements would have been required for these components to approach chemical and isotopic equilibrium. Experimentally derived, low-pressure metal-silicate distribution coefficients for the HSE are typically $>10^4$ (e.g., [Kimura et al., 1974](#); [Newsom, 1990](#); [O'Neill et al., 1995](#); [Borisov and Palme, 1995](#); [Fortenfant et al., 2003](#); [Brenan et al., 2016](#)). When metal-silicate equilibrium is achieved, the difference in abundances between metal and silicate for each HSE should reflect these large metal-silicate distribution coefficients ([Fig. 1d](#)). Further, the HSE in the silicates should be highly fractionated, relative to bulk chondrites, because of the variable metal-silicate distribution coefficients among the HSE ([Fig. 1d](#); [Brenan et al., 2016](#)). The concentrations of HSE in the nonmagnetic fractions for H4, H5, and H6 chondrites reported here, compared to their concentrations in the metals, are too high to reflect equilibrium between metals and silicates ([Fig. 1](#)). This observation is consistent with the data reported for H3.8 and H4 chondrites ([Horan et al., 2009](#)). Further, there is no correlation between metamorphic grade and HSE abundances of metals and nonmagnetic fractions.

It is conceivable the lack of apparent equilibration between metal and nonmagnetic fractions reflects incomplete removal of metal from the nonmagnetic fractions (e.g., [Chou et al., 1973](#)). Because of the low abundances of Pd in nonmagnetic fractions, metal/nonmagnetic

concentration ratios of Pd can be used to calculate a maximum possible quantity of metal contaminant in the nonmagnetic fractions ([Horan et al., 2009](#)). The lowest metal/nonmagnetic concentration ratio of Pd for the three H chondrites examined here of ~ 50 for ALHA 78115 indicates that any metal contaminant must comprise $<2\%$ of the nonmagnetic fraction. For Richardton, the metal/nonmagnetic Pd ratio is >2200 , indicating that metal contamination must comprise $<0.05\%$ of the nonmagnetic fraction. In addition, if the HSE abundances of the nonmagnetic fractions reflected the presence of metal contaminant, then the relative abundance patterns of metal and nonmagnetic fractions should be similar. However, the relative HSE abundances of the nonmagnetic fractions (especially Pd/Os) differ significantly from their respective metal fractions for the H chondrites investigated here, as well as for those investigated by [Horan et al. \(2009\)](#). Therefore, the comparatively high HSE abundances of H chondrite nonmagnetic fractions more likely reflect the presence of nonmetallic HSE-rich carriers, such as highly refractory condensates or residues of metal melting, which never equilibrated with the metal, as concluded by [Horan et al. \(2009\)](#). The HSE data reported here indicate that at even high degrees of metamorphism, the HSE carrier in the nonmagnetic fraction did not fully equilibrate with the metal.

Previous studies of H chondrites have observed that fine-grained metal fractions in H3.8-H4 chondrites have higher HSE abundances than their respective coarse-grained metal fractions (e.g., [Horan et al., 2009](#)). If equilibrium was achieved among metal grains during thermal metamorphism, fine- and coarse-grained metal fractions should have similar HSE abundances. However, the HSE concentrations of H4-6 fine-grained metal fractions from this study are significantly higher than those of their respective coarse-grained metal fractions ([Fig. 1](#)). Further, there is also no correlation between metamorphic grade and HSE abundance differences between fine- and coarse-grained metal. One possible explanation for this is that the metal fractions did not fully equilibrate, but coarse-grained metal fractions from the H4-6 chondrites examined in this study contain secondary, impact-derived metal nodules, which have HSE abundances that are lower than fine-grained metal, and highly fractionated relative to bulk chondrites ([Rubin, 1999](#)). The relative abundances of HSE in the coarse-grained metal fractions from the H chondrites examined here are unfractionated, relative to bulk chondrites, however, so the presence of coarse-grained impact-generated metal nodules cannot account for the difference in HSE abundances. Another possibility is that different surface area/volume ratios and localized equilibration resulted in higher HSE abundances within the fine-grained metal fraction, as argued below to explain different W isotopic compositions of fine- and coarse-grained metal (see [Section 5.5](#) for further discussion of disequilibrium among metal fractions). Regardless of the cause, the HSE data for metal fractions reported here indicate that, even following comparatively high degrees of thermal metamorphism, metal grains were not fully equilibrated. Diffusion of HSE among metal grains must have therefore been variable and inefficient, even at peak metamorphic temperatures.

Metal-silicate distribution coefficients for W are also typically high (>100) under low-pressure and temperature conditions (e.g., Wade and Wood, 2005). Except for Avanhandava, the H chondrites examined here have differences in W concentrations between magnetic and nonmagnetic fractions that are within the range expected for metal-silicate equilibration. However, the partitioning behavior of W is highly dependent on both intensive and extensive parameters (including pressure, temperature, metal compositions, silicate compositions, and fO_2), and experimentally-determined metal-silicate distribution coefficient vary by over two orders of magnitude (e.g., Cottrell et al., 2009) and are, at this time, only available for high T conditions more relevant to terrestrial core formation. It is therefore unclear whether the distribution of W among H chondrite components reflects complete metal-silicate equilibration. Future experimental work investigating W diffusion under more appropriate metamorphic conditions is necessary to further assess the degree of metal-silicate equilibration during thermal metamorphism on the H chondrite parent body.

5.3. H chondrite Hf-W isochrons and metal model ages

Chondrite component fractions with variable Hf/W will form an isochron on a plot of $^{180}\text{Hf}/^{184}\text{W}$ vs. $^{182}\text{W}/^{184}\text{W}$, if the following conditions are met: (i) all components were initially in isotopic equilibrium at the time of system closure (i.e., shared a common $^{182}\text{W}/^{184}\text{W}$), and (ii) the system was not subsequently disturbed. The slightly magnetic and nonmagnetic fractions of most chondrites examined here define precise isochrons (Fig. 4a, b, and e), however, the respective metal fractions of these chondrites plot below the isochrons, except for the <150 μm metal fractions from Richardton and Forest City (Fig. 4c and d). Thus, most metals were either not in equilibrium with silicate-rich fractions at the times of system closure recorded by the silicate-rich fractions, or the metals were subsequently disturbed.

The Hf-W closure ages, calculated from the slopes of linear regressions of only the slightly magnetic and nonmagnetic fractions (i.e., no metal fractions included), in comparison to CAI, are provided in Table 4 and Fig. 5a. Of note, the Hf-W closure age of Oakley (H6) is the youngest (15.2 ± 1.0 Ma) and Richardton (H5) the oldest (5.2 ± 1.6 Ma), although its age is within uncertainties of other H5 chondrites. Avanhandava (H4) has a closure age of 8.7 ± 1.7 Ma that is similar to the closure ages of the H5 chondrites reported here. The limited spread in $^{180}\text{Hf}/^{184}\text{W}$ (from 2.99 to 3.14) for ALHA 78115 nonmagnetic and slightly magnetic fractions results in a slope that is not meaningful. Consequently, the age of 23.7 ± 2.6 Ma before CAI formation should not be interpreted to have age significance. The well-resolved isotopic differences between the nonmagnetic and slightly magnetic fractions for this meteorite most likely indicate either that the two fractions were not in isotopic equilibrium at the time of complete system closure, or that the fractions experienced different degrees of open-system behavior.

The metal fractions for all of the H chondrites have low Hf/W ratios, so their $\epsilon^{182}\text{W}$ values approximate the initial $\epsilon^{182}\text{W}$ values of the metal when diffusive exchange of W

with surrounding silicates ceased. Correction for radiogenic ingrowth of ^{182}W is insignificant (<5 ppm), even for the metal fractions with the highest Hf/W ratios. Two stage metal model ages of diffusive cessation are calculated using the following equation:

$$\Delta t_{\text{CAI}} = -\frac{1}{\lambda} \times \ln \left[1 - \frac{\epsilon^{182}\text{W}_{\text{Metal}} - \epsilon^{182}\text{W}_{\text{Chondrite}}}{\epsilon^{182}\text{W}_{\text{CAI}} - \epsilon^{182}\text{W}_{\text{Chondrite}}} \right] \quad (2)$$

where $\epsilon^{182}\text{W}_{\text{Metal}}$ is the measured $\epsilon^{182}\text{W}$ of the metal, $\epsilon^{182}\text{W}_{\text{CAI}}$ is the currently accepted $\epsilon^{182}\text{W}_i$ of CAIs (-3.49 ± 0.07), which represents the Solar System initial value of $\epsilon^{182}\text{W}$ (Kruijer et al., 2014b), and $\epsilon^{182}\text{W}_{\text{Chondrite}}$ is the $\epsilon^{182}\text{W}$ value of the bulk H chondrite. For Richardton, a measured $\epsilon^{182}\text{W}_{\text{Chondrite}}$ of -2.79 for the bulk meteorite was reported by Kleine et al. (2008). However, measured $\epsilon^{182}\text{W}_{\text{Chondrite}}$ values are currently unavailable for all other H chondrites examined here, and so the average value for H chondrites (-2.3), calculated from Kleine et al. (2007), was used instead. Given the range of H chondrite $\epsilon^{182}\text{W}_{\text{Chondrite}}$ values (-2.8 to -2.0) reported by Kleine et al. (2007), the use of an average value for H chondrites introduces significant errors into model ages. In addition, two-stage model ages rely on the assumption that the Hf/W of the assumed chondritic reservoir remained constant since the time of CAI formation. However, it is possible that chondritic reservoirs were fractionated between the time of CAI formation and parent body accretion (Hellmann et al., in preparation). Therefore, these model ages have less certain chronological meaning than the isochron ages. The resulting model ages range from 1.4 ± 0.8 Ma, for one Richardton metal fraction, to 12.6 ± 0.9 Ma for one Forest City metal fraction (Table 5 and Fig. 5b). Fine-grained metal from Richardton and Forest City appear to be co-isochronous with their respective, slightly- and nonmagnetic fractions, and have model ages that are younger than their respective, metal-free isochron ages. By contrast, the differences between the model ages for most of the metal fractions and their respective, younger isochron ages for slightly- and non-magnetic fractions indicates that not all components were initially in isotopic equilibrium at the time of total system closure, were subsequently disturbed, or both.

5.4. H chondrite metal-silicate disequilibrium

One possibility for the observed non-isochronous ^{182}Hf - ^{182}W behavior of >150 μm metal fractions with non-magnetic and slightly magnetic fractions is that these fractions were disturbed by terrestrial alteration. However, the ^{187}Re - ^{187}Os systematics of >150 μm metal fractions plot within uncertainties of a primordial reference isochron (see Section 5.1), indicating closed system behavior of these fractions even for Re and Os, which are susceptible to redistribution on the order of a few percent during terrestrial alteration. Further, the high W concentrations and the low abundances of Hf in the metal suggest that alteration was unlikely to have affected the Hf-W systematics of the metal fractions. Finally, most metal fractions plot below their respective isochrons rather than above, as would be expected for open-system behavior caused by terrestrial

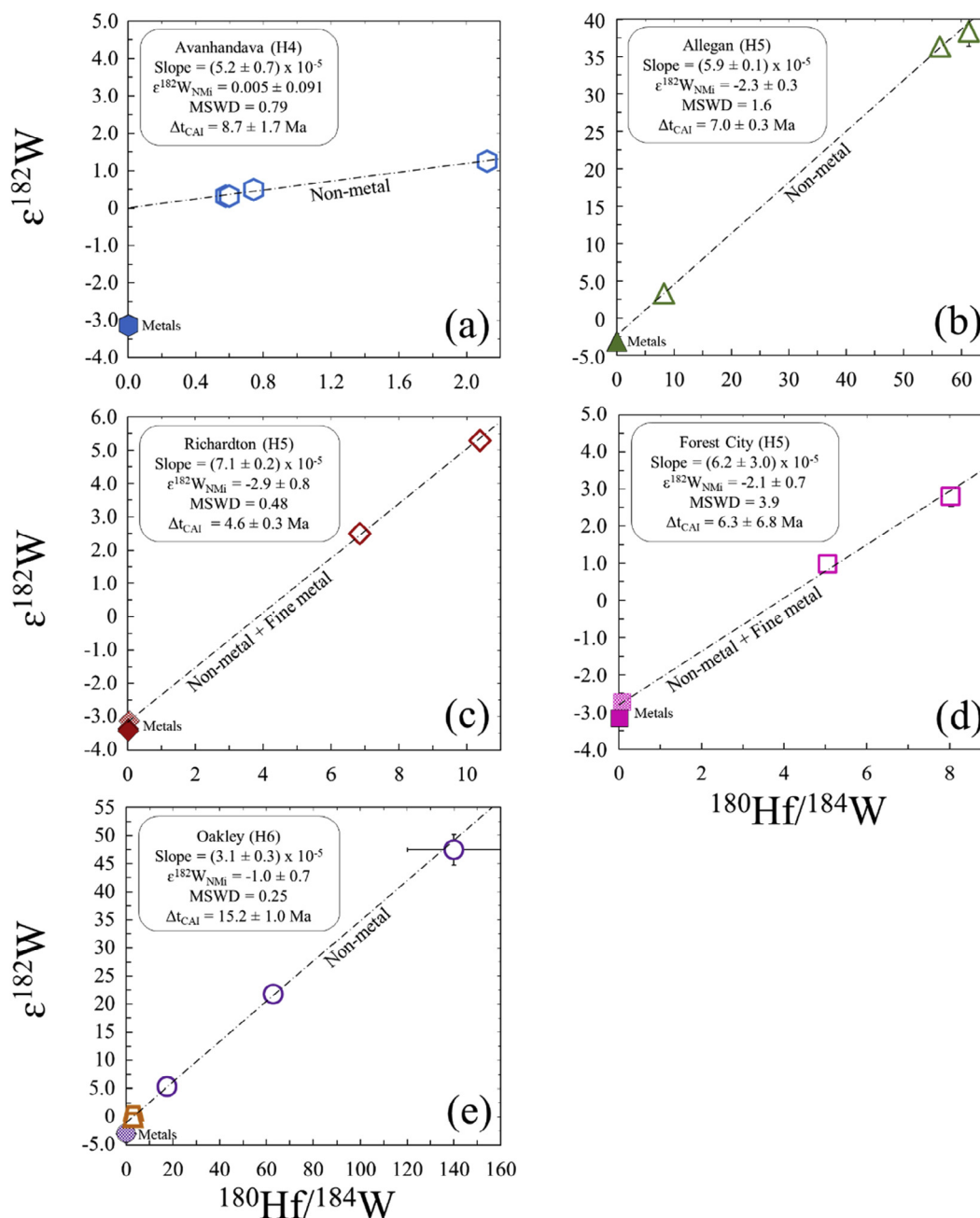


Fig. 4. $^{180}\text{Hf}/^{184}\text{W}$ vs. $\epsilon^{182}\text{W}$ for: (a) Avanhandava (H4), (b) Allegan (H5), (c) Richardton (H5), (d) Forest City (H5), and (e) Oakley (H6; purple) and ALHA 78115 (H6; brown) $>150\ \mu\text{m}$ metal (solid filled symbols), $<150\ \mu\text{m}$ metal (shaded symbols), and slightly magnetic and nonmagnetic fractions (open symbols). Isochrons shown are the linear regressions of data from each meteorite determined using ISOPLOT (Ludwig, 2001). Metal fractions are not included in the linear regressions for a, b, and e. The non-metal and $<150\ \mu\text{m}$ metal fractions are included in linear regressions of c and d. No fractions from ALHA 78115 are included in the linear regression of e.

Table 4

Hafnium-W isochron slopes, closure ages, and initial $\epsilon^{182}\text{W}$ of H chondrites calculated from regressions of slightly- and non-magnetic fractions. Δt_{CAI} is the closure age relative to CAIs. $\epsilon^{182}\text{W}_{\text{NMI}}$ is the calculated initial $\epsilon^{182}\text{W}$ value. Slope = initial $^{182}\text{Hf}/^{180}\text{Hf}$ value.

H Chondrite	Slope	2σ	Δt_{CAI}	2σ	$\epsilon^{182}\text{W}_{\text{NMI}}$	2σ
Avanhandava NM + SM (H4)	5.2×10^{-5}	0.7×10^{-5}	8.7 Ma	1.7 Ma	0.005	0.09
Allegan NM + SM (H5)	5.9×10^{-5}	0.1×10^{-5}	7.0 Ma	0.3 Ma	-2.3	0.3
Forest City NM + SM (H5)	5.3×10^{-5}	0.9×10^{-5}	8.4 Ma	2.3 Ma	-2.1	0.7
Richardton NM + SM (H5)	6.8×10^{-5}	0.8×10^{-5}	5.2 Ma	1.6 Ma	-2.9	0.8
Oakley NM + SM (H6)	3.1×10^{-5}	0.3×10^{-5}	15.2 Ma	1.0 Ma	-1.0	0.7

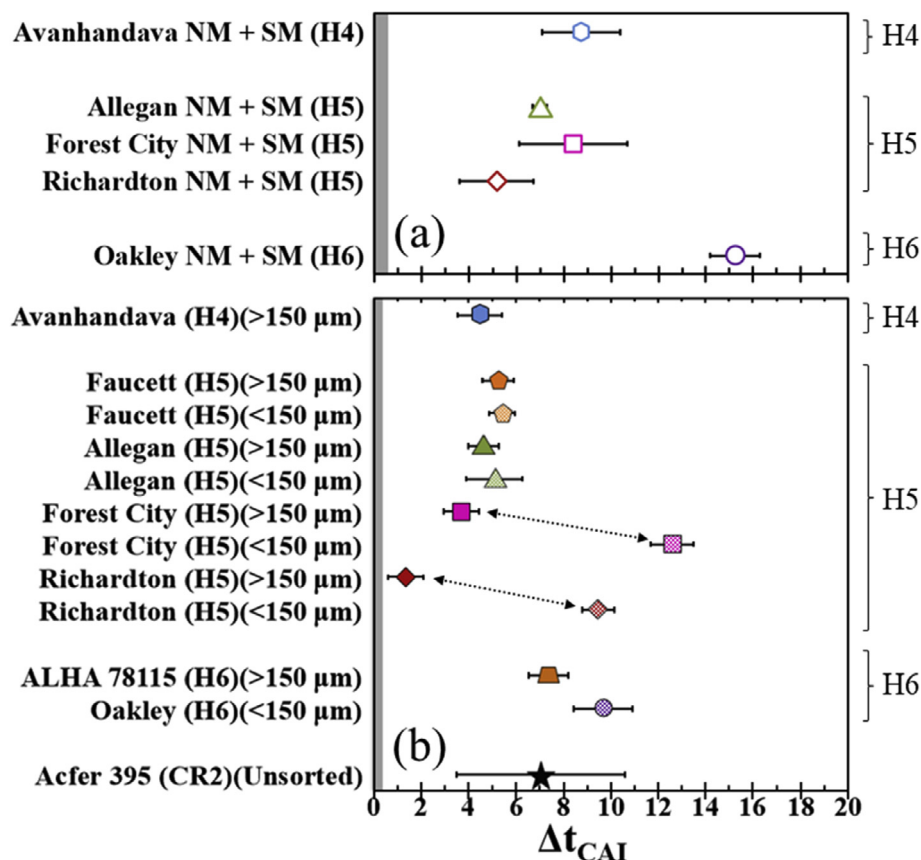


Fig. 5. Hafnium-W ages for H and CR chondrites, in Ma since CAI formation. (a) Slope-derived ages for linear regressions of H chondrite nonmagnetic and slightly magnetic fractions (open symbols). (b) Model ages for H chondrite >150 μm (solid fill) and <150 μm (shaded) metal fractions, calculated by comparing the $\epsilon^{182}\text{W}$ of each metal fraction to the $\epsilon^{182}\text{W}$ of bulk chondrites and the $\epsilon^{182}\text{W}_i$ of CAIs (Eq. (2)). The model age for Acfer 395 metal has been corrected for nucleosynthetic effect using the $\epsilon^{183}\text{W}$ value. Grey bars are the 2SE uncertainty for $\Delta t_{CAI} = 0$, calculated using the reported uncertainties for the CAI initial $^{182}\text{Hf}/^{180}\text{Hf}$ and $\epsilon^{182}\text{W}$ for (a) and (b), respectively (from Kruijer et al., 2014b).

Table 5

Model ^{182}W ages for H and CR chondrite metal fractions (in Ma since CAI formation). The model age for Acfer 395 metal has been corrected for nucleosynthetic effects (see Section 5.8).

Metal fraction	Model age Δt_{CAI}	2 σ
Avanhandava (H4) (>150 μm)	4.5	0.9
Faucett (H4) (>150 μm)	5.3	0.6
Faucett (H4) (<150 μm)	5.4	0.5
Allegan (H5) (>150 μm)	4.6	0.6
Allegan (H5) (<150 μm)	5.1	1.2
Forest City (H5) (>150 μm)	3.7	0.7
Forest City (H5) (<150 μm)	12.6	0.9
Richardton (H5) (>150 μm)	1.4	0.8
Richardton (H5) (<150 μm)	9.5	0.7
ALHA 78115 (H6) (>150 μm)	7.4	0.8
Oakley (H6) (<150 μm)	9.7	1.2
Acfer 395 (CR2) (Unsorted)	7.0	3.6

weathering. The minimal scatter about the isochrons for the slightly magnetic and nonmagnetic fractions of individual H chondrites, coupled with their Hf-W closure ages (5–15 Ma after CAI formation), which are broadly similar

to the range of previously reported Hf-W closure ages for H chondrites (Kleine et al., 2008; see additional comparison in Section 5.6), indicate that the Hf-W systematics of these fractions were also not significantly disturbed as a result of open system behavior caused by terrestrial weathering. Given the observed minor disturbance in ^{187}Re - ^{187}Os systematics of nonmagnetic fractions, ^{182}Hf - ^{182}W systematics of silicates-oxides must be less susceptible to redistribution by terrestrial alteration. This is consistent with observations made by previous studies that ^{187}Re - ^{187}Os systematics of Allende CAIs typically reflect secondary alteration processes (Archer et al., 2014), whereas the ^{182}Hf - ^{182}W systematics of Allende CAIs appear to reflect CAI formation (Kruijer et al., 2014b). Combined, these observations suggest that late-stage alteration is unlikely to be the cause of the non-isochronous behavior of most metal fractions versus silicate/oxide fractions, and in general, that ^{182}Hf - ^{182}W systematics are less susceptible to terrestrial alteration than ^{187}Re - ^{187}Os systematics. Therefore, the ^{182}Hf - ^{182}W characteristics more likely reflect differing efficiencies of W diffusion between oxides and silicates, as compared to diffusion between oxides-silicates and most metals.

Although there has not yet been an experimental study to explore W isotopic exchange between metals and silicates, some prior studies have explored W diffusion in H chondrites and other materials that are geochemically relevant to H chondrites. For example, [Humayun and Campbell \(2002\)](#) measured W and other siderophile element abundances in H chondrite metal grains of different petrologic types (H3–6). The *in situ* analytical technique they applied allowed the authors to investigate siderophile element abundances of individual metal grains of varying size, major element compositions, and petrographic context. They reported that the W/Ir of H chondrite metal grains increases with increasing petrologic type, up to H5, so that $H3 < H4 < H5 = H6$. They interpreted this increase as evidence for W diffusion from the matrix to metal. However, [Humayun and Campbell \(2002\)](#) also reported heterogeneous W abundances among H5 and H6 chondrite metal grains. For example, they reported W abundances for Keronouve (H6) kamacite grains that range from ~ 800 to >5000 ppb. Therefore, even at high degrees of thermal metamorphism, W was not fully equilibrated among metal grains. This observation is consistent with the lack of HSE equilibration among metal grains.

[Cherniak and Van Orman \(2014\)](#) reported experimental data for W diffusion in olivine over a range of temperatures and fO_2 conditions relevant to H chondrites. Using these data, they modeled diffusive loss of W from olivine into metal over a range of conditions. Of particular relevance to this study, they modeled the diffusive transport of W from olivine to metal following presumed multi-stage cooling during fragmentation and re-accretion of the H chondrite parent body, as proposed by [Ganguly et al. \(2013\)](#). In their three-stage model, H chondrites initially cool from peak temperatures of ~ 750 to ~ 850 °C, at 50 °C/ka. During a second stage, H5 and H6 chondrites cool more slowly at 15 °C/Ma. In a final stage, H6 chondrites cool at 3 °C/Ma. [Cherniak and Van Orman \(2014\)](#) argued that during such a cooling history, H4 chondrite olivine grains would undergo less than 2% loss of W, even for the smallest grains (1–2 μm). Small olivine grains (~ 2 μm radius) in the H5 and H6 chondrites would lose 17% and 18% of their W, respectively, while olivine grains that were 50 μm and larger would lose $<1\%$. It should be noted, however, that olivine is not a major carrier of either Hf or W in H chondrites, so the experimental data from [Cherniak and Van Orman \(2014\)](#) only highlight the possibility that W retention by silicates/oxides may have played a role in the disequilibrium between metal grains and silicates/oxides.

[Yokoyama et al. \(2009\)](#) reported experimental data for chemical equilibration and isotopic exchange of Os, a HSE, between iron meteorites and basalts under high pressure and temperature conditions. They reported that despite the apparently efficient diffusion of Os from silicates to metal nuggets, complete isotopic equilibration did not occur. They interpreted this to indicate that isotopic exchange occurred at a slower rate than chemical equilibration under their experimental conditions. Osmium, however undoubtedly differs from W in metal-silicate diffusion rates. A study using a similar experimental design to that of

[Yokoyama et al. \(2009\)](#) could be useful for exploring isotopic exchange of W among H chondrite components.

5.5. Disequilibrium of metal fractions

In contrast to the other H chondrites studied, the >150 μm and <150 μm metal grains from Faucett and Allegan have similar $\epsilon^{182}\text{W}$ values, within uncertainty. Therefore, the metal grain fractions in these two meteorites may have reached and maintained equilibrium with each other on the parent body. By contrast, the higher $\epsilon^{182}\text{W}$ values for some <150 μm metal fractions, compared to their respective >150 μm metal fractions in the other H chondrites studied, indicate that some metal grains from individual chondrites were not in equilibrium with each other following complete cessation of diffusive exchange of W among chondrite components. It is possible that in these meteorites the <150 μm metal grains continued to efficiently exchange W with surrounding silicates/oxides at lower temperatures than >150 μm metal grains, possibly due to having larger surface area to volume ratios. Another possibility is that grain boundary diffusion resulted in less efficient diffusion of W from silicates/oxides to coarse-grained metal than fine-grained metal, even when both <150 μm and >150 μm metal grains were above their respective Hf-W closure temperatures.

[Quitté et al. \(2005\)](#) modeled lattice diffusion of W through metal and silicates during thermal metamorphic conditions, and showed that diffusion in silicates occurs at smaller length scales than in metals at the given thermal conditions for mesosiderites and pallasites, during cooling on their respective parent bodies. Using previously reported diffusion parameters for W diffusion in metal ([Jost 1960](#)), olivine ([Cherniak and Van Orman 2014](#)), and high Ca-pyroxene ([Kleine et al., 2008](#)), we calculated diffusion distances of W within these phases during cooling of the H chondrite parent body (see electronic annex). For example, assuming a cooling rate of 10 °C/Myr for H6 chondrites ([Kleine et al., 2008](#)), calculated W diffusion distances for high Ca-pyroxene and olivine diminish to <0.5 mm below 900 °C and 910 °C, respectively. At 880 °C, only 5 °C above the Hf-W closure temperature of H6 chondrites, calculated W diffusion distances are only ~ 0.3 mm for both olivine and high-Ca pyroxene. Therefore, as H chondrites approached their Hf-W closure temperatures, equilibration became progressively more localized. As >150 μm metal grains contain greater volumes of metal and higher total abundances of W, localized equilibration likely resulted in only limited overprinting of the original W isotopic compositions of >150 μm metal grains. By contrast, smaller metal grains would have been more easily overprinted during localized equilibration, because of their smaller volumes and lower total abundances of W. Therefore, traditional lattice diffusion at progressively lower temperatures may account for at least some of the variability in W isotopic compositions among H chondrite metal grains. We note that it is possible, albeit not required, that <150 μm metal and >150 μm metal reached equilibrium at some point, and then subsequent diffusion of radiogenic W to

<150 μm metal grains during cooling resulted in differential abundances of ^{182}W .

In addition to lattice diffusion, grain-boundary diffusion of W could also have played a role in producing isotopic disequilibrium among different metal grains. [Hayden and Watson \(2007\)](#) reported experimental results for grain-boundary diffusion of highly and moderately siderophile elements (including W) through polycrystalline MgO. Under high pressure and temperature conditions, siderophile elements were transported from initially siderophile element enriched ‘source’ metal particles to initially siderophile element depleted ‘sink’ metal particles through grain-boundary pathways. There are several reasons why the experimental data from [Hayden and Watson \(2007\)](#) are particularly relevant to H chondrites. First, as W is incompatible in the silicate/oxide phases of H chondrites, grain boundaries were likely to be the primary pathway for W diffusion, rather than lattice diffusion. Second, like the experimental setup, siderophile elements were initially heterogeneously distributed among metal grains in H chondrites (i.e., prior to thermal metamorphism; [Humayun and Campbell, 2002](#)), indicating that grain boundary diffusion between metal grains was required to approach equilibrium. Finally, even though high Ca-pyroxene also acted as a ‘source’ phase in H chondrites, in addition to metal, grain boundary diffusion was still the primary pathway for W diffusion from that source.

Of importance to this study, [Haydon and Watson \(2007\)](#) reported that ‘sink’ metal particles from individual experiments received disproportionate amounts of siderophile elements, indicating variations of diffusion efficiencies through different grain boundary pathways. They argued that grain coarsening of the polycrystalline MgO during experimental runs, which decreased grain-boundary areas and altered or removed grain-boundary pathways, was associated with a decrease in the diffusion of siderophile elements from ‘source’ particles. They also reported that ‘sink’ metal closer to ‘source’ metal received greater proportions of siderophile elements and effectively shielded ‘sink’ metal farther away.

The experimental results of [Hayden and Watson \(2007\)](#) support disproportionate grain boundary diffusion as one likely mechanism that contributed to the variability in W isotopic compositions among H chondrite metal grains. In H chondrites, disproportionate diffusion may have been the result of several different processes. First, <150 μm metal grains may be spatially associated with finer-grained silicates/oxides, and therefore, higher densities of grain boundaries and lattice defects than >150 μm metal grains, which resulted in more efficient diffusion pathways and higher fluxes of radiogenic W to <150 μm metal grains. Second, metal grains <150 μm in size may also be more often located closer to the sources of radiogenic W, high Ca pyroxene and ilmenite ([Righter and Shearer, 2003](#)), and they may have effectively shielded >150 μm metal grains from incorporation of radiogenic ^{182}W . Finally, disproportionate diffusion may have occurred because of the larger volumes of coarse-grained metal, and the effective metal shielding described by [Hayden and Watson \(2007\)](#). Metal grain shielding would have resulted in localized

equilibration between metals and silicates/oxides, rather than bulk-scale equilibration.

The aforementioned possibilities are not mutually exclusive, and each, or a combination of them, can potentially account for different $\epsilon^{182}\text{W}$ values for >150 μm versus <150 μm metal grains. There currently are not sufficient experimental data to assess this issue further. In addition, as stated above, some H chondrites do not show a clear difference in $\epsilon^{182}\text{W}$ values between >150 μm and <150 μm metal grains, whereas other H chondrites do. Future work, combining diffusion experiments with isotopic analyses of metal fractions with more diverse grain sizes (i.e., more than 2 grain sizes), will be required to provide further constraints on the true cause(s) of non-isochronous behavior and variable W isotopic compositions of H chondrite metal grains.

5.6. Onion-shell structure of the H chondrite parent body?

In the onion-shell thermal model (e.g., [Pellas and Storzer, 1981](#); [Trieloff et al., 2003](#)), the H4 chondrites either reached the closure temperature for any given thermochronological system (e.g., Ar-Ar) earlier than H5 and H6 chondrites, as they were the fastest to cool, or they were never heated to temperatures above the closure temperature, as proposed by [Kleine et al. \(2008\)](#) for the Hf-W thermochronometer. In either case, the H4 chondrites should record the oldest closure ages. The H6 chondrites reached the highest peak temperatures, cooled the slowest, and, therefore, should record the youngest closure ages.

The onion-shell thermal model has largely been based upon evidence from members of a suite of nine H chondrites originally measured by [Pellas and Storzer \(1981\)](#) for ^{244}Pu fission closure ages, and [Trieloff et al. \(2003\)](#) for both Ar-Ar and ^{244}Pu fission track closure ages. Subsequent studies (e.g., [Kleine et al., 2008](#); [Harrison and Grimm, 2010](#); [Henke et al., 2012](#); [Monnereau et al., 2013](#)) focused on the same suite of H chondrites to build a consistent, comprehensive thermochronometric dataset. Of the five H chondrites examined by [Kleine et al. \(2008\)](#) for Hf-W isotopic systematics, four were from the same suite of H chondrites examined by [Trieloff et al. \(2003\)](#). They reported that the H chondrite metal-silicate data produced precise Hf-W isochrons within the $\pm 0.3\text{--}0.4 \epsilon$ unit external precision of their measurements, and that metals and silicates appeared to have been in equilibrium at the time of system closure. They also reported an inverse correlation between metamorphic grades and Hf-W closure ages, consistent with the onion-shell thermal model. The least metamorphosed H chondrite examined by that study, Ste. Marguerite (H4), had the oldest Hf-W closure age (1.7 ± 0.7 Ma after CAI formation), and the most metamorphosed H chondrites, H6 chondrites Estacado and Kernouvé, had the youngest ages (combined, 9.6 ± 1.0 Ma after CAI formation). [Kleine et al. \(2008\)](#) combined the Hf-W data with previously reported closure ages for other systems with varying closure temperatures (Pb-Pb, Ar-Ar, ^{244}Pu fission tracks) for the same samples to produce cooling rate curves for different portions of the H chondrite parent body. Supporting the onion-shell model, the H4 chondrites cooled the

fastest (55 °C/Ma), and the H6 chondrites cooled slowest (~10 °C/Ma).

Of the H chondrites examined here, the H6 chondrite Oakley has the youngest isochron closure age of all samples (Fig. 5a). The H5 chondrites Allegan and Forest City have closure ages that are similar to each other and older than the H6 chondrite Oakley. The H5 chondrite Richardton appears to have a slightly older age than Allegan and Forest City, however secondary processes may have modified Richardton, and it may not have originated from the same parent body (see Section 5.7). The H4 chondrite Avanhandava has an age that is similar to those of the H5 chondrites Allegan and Forest city, and younger than Richardton (H5).

The H5 chondrite Richardton was measured in this study and by Kleine et al. (2008). The closure ages determined are similar, with 5.6 ± 1.1 Ma and 5.2 ± 1.6 Ma for Kleine et al. (2008) and this study, respectively. However, the nonmagnetic and slightly magnetic fractions from the two studies, when regressed together, do not form a precise isochron (MSWD = 5.6). This discrepancy may be the result of the lower blank corrections of this study (see Section 3.1), or differential modification of ^{182}W by cosmic rays (see section 5.7), which has been previously observed within different pieces of the same meteorite (e.g., Markoswi et al., 2006a). As discussed in section 5.3, combined H chondrite metal-silicate data from this study do not form precise Hf-W isochrons for most H chondrites. The lack of isochronous behavior for all fractions differs from the findings of Kleine et al. (2008), but is probably the result of the improved analytical precision and lower, and therefore more precise, blank corrections of this study. This makes comparisons of isochron ages between the two studies problematic.

The H6 chondrite Oakley is ~5 Ma younger than the H6 chondrites reported by Kleine et al. (2008). The H5 chondrites Allegan and Forest City have closure ages that appear to be slightly younger than the H5 chondrites reported by Kleine et al. (2008), although they are within uncertainties. The closure age of Avanhandava is ~7 Ma younger than the closure age of the H4 chondrite Ste. Marguerite measured by Kleine et al. (2008). However, Ste. Marguerite has been identified as an anomalous H4 chondrite by Scott et al. (2014), as it has a metallographic cooling rate $>10,000$ °C/Myr, which cannot be generated during cooling in an onion-shell thermal structure. As for the other H chondrites, the general differences between ages reported here and by Kleine et al. (2008) is likely the result of a bias caused by inclusion of non-isochronous metal fractions in the isochrons of Kleine et al. (2008). We therefore only consider the more precise data reported here in assessing the onion-shell thermal model.

Consistent with previous studies supporting an onion-shell model, the observation that the Hf-W isochron ages of H5 and H6 chondrites reported here are all inversely correlated with metamorphic grades supports an onion-shell thermal model (Fig. 5a). By contrast, the lack of substantial variation in Hf-W isochron ages for Avanhandava (H4) and the H5 chondrites reported here are inconsistent with an onion-shell thermal model. Therefore, the H chondrites investigated by the study are mostly, but not completely, consistent with the onion-shell thermal model.

One possible model to explain the expanded Hf-W closure ages for H chondrites is a modified version of the onion-shell thermal model that also includes partial disruption of the outer portion of the H chondrite parent body (e.g., Harrison and Grimm, 2010; Blackburn et al., 2017). In this model, the H chondrite parent body accreted at ~2 Ma after CAI formation, and formed with a concentrically-zoned onion-shell thermal structure. The deeper portions of the parent body, from which H5 and H6 chondrites originated, remained undisturbed until they cooled below their respective Hf-W closure ages. The shallower portions of the H chondrite parent body, from which H4 chondrites originated, however, were continuously disrupted shortly after accretion by impacts.

The Hf-W data for H5 and H6 chondrites reported here are consistent with preservation of an onion-shell thermal structure, and therefore consistent with this model. By contrast, the data for the H4 chondrite reported here are inconsistent with an onion-shell thermal model. Instead, the comparatively young age for this H chondrite may reflect isotopic resetting either by reheating due to impacts, or excavation followed by reburial and reheating above the Hf-W closure temperature at ~9 Ma after CAI formation. We note that in the case of reheating after reburial, the H4 chondrite would have to have been reburied to a depth similar to the depths of burial of the H5 chondrites in order for sufficient reheating to reset the Hf-W system at ~9 Ma after CAI formation. In either case, the Hf-W data for this H4 chondrites is consistent with partial disruption of the shallowest portions of the H chondrite parent body, and consistent with this model.

The results of several prior studies support this modified onion-shell thermal model. Blackburn et al. (2017) reported that Pb-Pb ages for H5 and H6 chondrites are consistently inversely correlated with metamorphic grade, indicating that the portions of the parent body from which these samples originated remained undisturbed below the Pb-Pb closure age. However, they also reported a Pb-Pb closure age for Avanhandava (~60 Ma after CAI formation) that is too young to be consistent with an onion-shell thermal model. They argued that a disruption event that occurred around 60 Ma after CAI formation reheated some H4 chondrites, including Avanhandava, and re-buried them to depths within a rubble pile that were greater than their depths within the original, concentrically zoned H chondrite parent body. Blackburn et al. (2017) also argued that impact-driven erosion of the surface of the H chondrite parent body could account for early Pb-Pb closure ages (5–7 Ma after CAI formation) and fast metallographic cooling rates (10^3 – 10^4 °C/Ma; Scott et al., 2014) for some other H4 chondrites. Scott et al. (2014) reported metallographic cooling rates for some H4 chondrites of ≥ 5000 °C/Myr, which are ~50× higher than the highest cooling rates expected for the onion-shell thermal structure. They argued that these cooling rates must reflect excavation of H4 chondrites by impacts on the H chondrite parent body. Harrison and Grimm (2010) compared previously published closure ages and cooling rates with computational models for an onion-shell thermal structure, and found that an onion-shell thermal model could account for most, but not all, H

chondrites studied. In order to account for the subset of samples with closure ages and cooling rates that were inconsistent with an onion-shell thermal model, they argued for a ‘perturbed onion-shell model,’ in which the parent body was partially, but not completely, disturbed by impacts. Therefore, based on combined observations from Hf-W, Pb-Pb, metallographic cooling rate data, and thermal modelling, we conclude that much of the H chondrite parent body retained an onion-shell thermal structure, but the outer portion of the parent body from which H4 chondrites originated were continuously disturbed following accretion.

5.7. Richardton: an anomalous H chondrite

The $\epsilon^{182}\text{W}$ value of Richardton >150 μm metal reported here (-3.42 ± 0.09) is in good agreement with some values reported by a previous study (-3.47 ± 0.19 and -3.32 ± 0.19 ; [Kleine et al., 2008](#)), although a wide range of $\epsilon^{182}\text{W}$ values were reported for Richardton >150 μm metal by that study (-3.06 ± 0.18 to -3.47 ± 0.19). These metal fractions have the lowest $\epsilon^{182}\text{W}$ values of any H chondrite metal fractions, and are comparable to values reported for IIAB, IIIAB, and IVA magmatic iron meteorite groups ([Kruijjer et al., 2014a](#)). These metal data are, thus, inconsistent with the metal data from other H5 chondrites, as well as metal data for any other H chondrite examined in this study. Therefore, it is important to assess whether the $\epsilon^{182}\text{W}$ of Richardton metal solely reflects the early isolation of the metal from ^{182}Hf , or if it instead reflects another process. Prior studies have reported low $\epsilon^{182}\text{W}$ values in certain meteorites. Some anomalies are evidently the result of inheritance of W from carrier phases with presolar, mass-independent nucleosynthetic isotopic anomalies ([Burkhardt et al., 2012](#); [Kruijjer et al., 2014b](#); [Breton et al., 2015](#)). Other anomalies have been attributed to the burnout of ^{182}W by neutron capture reactions during cosmic ray exposure (e.g., [Kleine et al., 2005](#); [Markowski et al., 2006a,b](#)). These two processes can affect the relative abundances of W isotopes in different ways, and can be distinguished by examining $\epsilon^{182}\text{W}$ vs. $\epsilon^{183}\text{W}$ relations.

Excesses of nucleosynthetic *s*-process carriers result in correlated deficits of ^{183}W and ^{182}W , with a slope of 1.41 ± 0.06 when $\epsilon^{183}\text{W}$ is plotted vs. $\epsilon^{182}\text{W}$ ([Kruijjer et al., 2014b](#); [Burkhardt and Schönbacher, 2015](#)). If the low $\epsilon^{182}\text{W}$ of Richardton >150 μm fractions were caused by *s*-process carrier excesses, a corresponding deficit in ^{183}W would be expected. However, the measured $\epsilon^{183}\text{W}$ of -0.04 ± 0.08 is indistinguishable from the standards within uncertainties. Thus, we conclude that nucleosynthetic effects cannot account for the low $\epsilon^{182}\text{W}$ of Richardton.

[Kleine et al. \(2008\)](#) suggested that the low $\epsilon^{182}\text{W}$ of Richardton metal might be the result of cosmic irradiation-induced W isotope anomalies, which have been reported for iron meteorites (e.g., [Kruijjer et al., 2012](#)). These anomalies occur because of the burnout and production of W nuclides during neutron-capture reactions ([Markowski et al., 2006a,b](#)). While all W isotopes are affected by these reactions to varying degrees, the overall effect is a decrease in measured $\epsilon^{182}\text{W}$ ([Kleine et al., 2005](#)). Cosmogenic ^{182}W anomalies strongly correlate with

the isotopic abundances of Os and Pt ([Kruijjer et al., 2013](#); [Wittig et al., 2013](#)) that are also susceptible to modification during irradiation by cosmic rays. Therefore, Pt or Os isotopes can be used as dosimeters to identify cosmogenic effects and make corrections to $\epsilon^{182}\text{W}$ to determine a ‘pre-exposure’ $\epsilon^{182}\text{W}$. Although no prior studies have reported cosmogenic Os, Pt, or W effects in bulk chondrites or their components, the $\mu^{189}\text{Os}$ value ([Fig. 3](#)) of Richardton metal is consistent with minor neutron capture and burnout effects, as reported by previous studies for some iron meteorites ([Walker, 2012](#); [Wittig et al., 2013](#); [Qin et al., 2015](#)). The relation between $\mu^{189}\text{Os}$ values and $\epsilon^{182}\text{W}$ values allows cosmogenic ^{182}W anomalies to be corrected using empirically-derived slopes, which appear to be similar for different iron meteorite groups (e.g., [Worsham et al., 2017](#); [Qin et al., 2015](#)). For example, using the slope (1.5 ± 0.5) derived from IAB iron meteorites (main group, sLL, and sLM; [Worsham et al., 2017](#)), and the magnitude of the measured $\mu^{189}\text{Os}$ deficit, the pre-exposure $\epsilon^{182}\text{W}$ value of the Richardton >150 μm metal fraction (-3.3 ± 0.1) is within uncertainty of Forest City >150 μm metal. However, the $\mu^{189}\text{Os}$ - $\epsilon^{182}\text{W}$ correlation may be specific to different meteorite groups and their parent bodies, as iron and chondritic bulk compositions moderate neutrons differently. Therefore, this correction is not precise and can only serve to highlight the possibility of cosmic ray irradiation.

It is conceivable that the W and Os isotopic compositions of silicates and oxides were similarly affected by cosmic rays. When plotted together, the nonmagnetic and slightly magnetic fractions from Richardton reported here and by [Kleine et al. \(2008\)](#) do not form a single, precise isochron (MSWD = 5.6). One possibility is that the two different pieces of Richardton separately examined by [Kleine et al. \(2008\)](#) and this study experienced differential modification of ^{182}W by cosmic rays due to different degrees of shielding within the parent body. Such differences in cosmogenic W effects within the same meteorite on the cm scale have been reported previously (e.g., [Markowski et al., 2006a](#)). However, using the Os dosimeter to correct for such effects in the silicates and oxides would be challenging because of the low abundances of Os (~ 9 ppb) in the nonmagnetic fraction, and the relatively large quantity (75–100 ng) of Os required for a high-precision analysis. Future work is necessary to assess the magnitude of cosmogenic effects in Richardton silicates and oxides.

Prior studies have typically reported cosmogenic effects in W and Os in iron meteorites, some of which have experienced high neutron fluences, consistent with their old exposure ages (hundreds of Ma). The possible W and Os cosmogenic effects suggested here for Richardton metal would be surprising, given that most cosmic ray exposure (CRE) data indicate that chondrites have relatively low cosmic ray exposure ages (<100 Ma, and typically less than 50 Ma), compared to iron meteorites, and therefore should have negligible neutron capture effects. Consistent with these general observations, Richardton has a cosmic ray exposure age (23.4 Ma; [Graf and Marti, 1995](#)) that is considerably younger than iron meteorites with reported W cosmogenic effects (>60 Ma; [Kruijjer et al., 2012](#)), and within the normal range of H chondrites. Therefore, it

seems unlikely that Richardton experienced a single-stage irradiation history similar to most iron meteorites. Instead, a more complicated irradiation history must be envisioned. Because ^{182}W effects increase with depth (Markowski et al., 2006a), one possibility is that during an initial stage of irradiation, this sample was shielded at depth from primary cosmic rays (which determine the apparent exposure age), but not from thermal or epithermal neutrons, which result in ^{182}W burnout.

One additional complexity involving Richardton comes from Mo isotopes. Worsham et al. (2017) reported that H5 chondrites Allegan and Richardton have nucleosynthetic anomalies in $\mu^{97}\text{Mo}$, corresponding to *s*-process depletions, but that Richardton has a larger *s*-process depletion than Allegan. This likely reflects a genetic difference between Richardton relative to other H chondrites. If so, it could mean that Richardton formed on a different parent body and that thermochronological data for it should not be considered within the framework of data for other H chondrites. Alternatively, Richardton could have formed on an H chondrite parent body characterized by the heterogeneous distribution of Mo-rich *s*-process carrier phases that never fully equilibrated, which would be consistent with the general chemical and isotopic disequilibrium of siderophile elements observed by this study. For this scenario, thermochronological data for Richardton would be relevant to the cooling history of the H chondrite parent body.

Since the origin of Richardton is particularly murky, it is safest to omit thermochronological data for it when assessing the cooling history of the H chondrite parent body. It does, however, highlight the diversity of H chondrites, and the need for further expansion of the H chondrite thermochronological dataset.

5.8. Formation of CR2 chondrite metal

The measured $\epsilon^{182}\text{W}$ (normalized to $^{186}\text{W}/^{184}\text{W}$) of Acfer 395 metal is -2.11 ± 0.16 , which is much more radiogenic than the H chondrite metal fractions. Also, unlike the H chondrite metal fractions, the CR chondrite metal fraction has a positive $\epsilon^{183}\text{W}$ value, which is consistent with previously reported data for CR chondrite separates (Budde et al., 2018). Budde et al. (2018) argued that the positive $\epsilon^{183}\text{W}$ values were the result of nucleosynthetic effects. This complicates determining a precise formation age from $\epsilon^{182}\text{W}$, because $\epsilon^{182}\text{W}$ is likely also abnormal as a result of a nucleosynthetic effect. However, the measured $\epsilon^{183}\text{W}$ and the slope of the $\epsilon^{182}\text{W}$ - $\epsilon^{183}\text{W}$ correlation reported by Budde et al. (2016) for Allende components can be used to calculate a nucleosynthetic-corrected $\epsilon^{182}\text{W}$ value of -2.8 ± 0.2 for Acfer 395 metal, which overlaps within uncertainties of most H chondrites measured here. The calculated model age for the metal using the corrected $\epsilon^{182}\text{W}$ value is 7.0 ± 3.6 Ma (Table 5, Fig. 5b). Even after the large correction for a nucleosynthetic effect, the age does not overlap with CAI formation, indicating that CR chondrite metal did not form by direct condensation from nebular gas, as proposed by some previous studies of CR metal (e.g., Weisberg et al., 1993). Instead, the metal must have formed by a later process, such as reduction of FeO,

or localized evaporation followed by condensation during chondrule formation (e.g., Zanda et al., 1994; Connolly et al., 2001; Wasson and Rubin, 2010; Humayun, 2012).

Prior studies have suggested that the CR chondrites may share a genetic link with the primitive achondrite Tafassasset, based on Cr and O isotopic data (Göpel et al. 2009). However, in contrast to the ^{183}W anomalies reported here for CR chondrite metal, previously reported $\epsilon^{183}\text{W}$ values for Tafassasset metal range from -0.06 ± 0.17 to 0.02 ± 0.2 (Breton et al., 2015). These observations are inconsistent with a genetic link between Tafassasset and CR chondrites, and these meteorites most likely originated from different parent bodies.

6. CONCLUSIONS

The Hf-W systematics and HSE abundances of metal and silicate fractions indicate that diffusion of siderophile elements among H chondrite components was limited. There is no clear correlation between metamorphic grade and extent of HSE equilibration. Combined metal-silicate Hf-W data do not form precise linear regressions for most H chondrites. Some size-sorted metal fractions have different W isotopic compositions and HSE abundances, indicating that some metal fractions were not in equilibrium when diffusive exchange of siderophile elements ceased. Most metal fractions plot below linear regressions of nonmagnetic and slightly magnetic fractions, indicating that equilibration between silicate/oxide phases and metal may have been incomplete. Combined metal-silicate Hf-W data, therefore, do not have clear chronological meaning for most H chondrites. By contrast, the slightly magnetic and nonmagnetic fractions form precise isochrons for most H chondrites, and therefore provide chronological evidence for the thermal history of the H chondrite parent body or bodies.

The Hf-W data for H5 and H6 chondrites reported here are consistent with an undisturbed onion-shell thermal model for the deeper portions of the H chondrite parent body. However, the Hf-W data for the H4 chondrite Avandava are more consistent with disruption of shallower portions of the H chondrite parent body, likely by impact. This scenario is supported by previously published Pb-Pb ages (Blackburn et al. 2017), metallographic cooling rates (Scott et al. 2014), and computational modelling (Harrison and Grimm, 2010) of H chondrites.

Metal from Richardton (H5) has the lowest $\epsilon^{182}\text{W}$ of any H chondrite measured here. Richardton metal also has different Os and Mo (Worsham et al., 2017) isotopic compositions from other H chondrite metal fractions. Richardton metal may have therefore experienced a large neutron fluence, modifying the W and Os isotopic compositions. Further, the Mo isotopic compositions (Worsham et al., 2017) indicate that Richardton may sample material that has a different population of nucleosynthetic *s*-process carrier phases, either because of heterogeneities on the H chondrite parent body, or because Richardton formed on a separate parent body.

The W isotopic composition of metal from CR chondrite Acfer 395 is consistent with a nucleosynthetic *s*-process depletion. The nucleosynthetic-corrected model

age for Acfer 395 does not overlap with CAI formation, and therefore the metal does not appear to have formed by condensation from nebular gas. Instead, CR chondrite metal must have formed by a later process.

ACKNOWLEDGEMENTS

We gratefully acknowledge the Smithsonian Institution National Museum of Natural History, the University of California Los Angeles Meteorite Collection and the Carnegie Institution for Science for providing the samples used in this study. Thorsten Kleine is especially thanked for guidance and valuable feedback. John Wasson and Alan Rubin are thanked for providing sufficient quantities of Acfer and Faucett, as well as helpful discussion. Conel Alexander, James Farquhar, Bill McDonough, Richard Ash, Katherine Bermingham, Emily Worsham, Mathieu Touboul, and Greg Brennecke are thanked for providing valuable feedback about this project. Igor Puchtel is thanked for providing help in the lab. We thank Alex Ruzicka, Ghylaine Quitté, an anonymous reviewer, and associate editor Maud Boyet for their thorough and constructive reviews. Partial funding for this work was provided by NASA Cosmochemistry grant NNX13AF83G and NASA Emerging Worlds grant NNX16AN07G (to RJW).

APPENDIX A. SUPPLEMENTARY MATERIAL

Supplementary data to this article can be found online at <https://doi.org/10.1016/j.gca.2018.11.012>.

REFERENCES

- Allègre C. M. and Luck J.-M. (1980) Osmium isotopes as petrogenetic and geological tracers. *Earth Planet. Sci. Lett.* **48**, 148–154.
- Archer G. J., Ash R. D., Bullock E. S. and Walker R. J. (2014) Highly siderophile elements and ^{187}Re – ^{187}Os isotopic systematics of the Allende meteorite: evidence for primary nebular processes and late-stage alteration. *Geochim. Cosmochim. Acta* **131**, 402–414.
- Archer G. J., Mundl A., Walker R. J., Worsham E. A. and Bermingham K. R. (2017) High precision analysis of $^{182}\text{W}/^{184}\text{W}$ and $^{183}\text{W}/^{184}\text{W}$ by negative thermal ionization mass spectrometry: per-integration oxide corrections using measured $^{18}\text{O}/^{16}\text{O}$. *Int. J. Mass Spectrom.* **414**, 80–86.
- Becker H., Morgan J. W., Walker R. J., MacPherson G. L. and Grossman J. N. (2001) Rhenium–osmium systematics of calcium–aluminum-rich inclusions in carbonaceous chondrites. *Geochim. Cosmochim. Acta* **65**, 3379–3390.
- Birck J. L., Barman M. R. and Capmas F. (1997) Re–Os isotopic measurements at the femtomole level in natural samples. *Geostand. Newsl.* **21**, 19–27.
- Blackburn T., Alexander M. O'D. C., Carlson R. W. and Elkins-Tanton L. T. (2017) The accretion and impact history of the ordinary chondrite parent bodies. *Geochim. Cosmochim. Acta* **200**, 201–217.
- Borisov A. and Palme H. (1995) The solubility of iridium in silicate melts: new data from experiments with $\text{Ir}_{10}\text{Pt}_{90}$ alloys. *Geochim. Cosmochim. Acta* **59**, 481–485.
- Brandon A. D., Puchtel I. S., Walker R. J., Day J. M. D., Irving A. J. and Taylor L. A. (2012) Evolution of the martian mantle inferred from the ^{187}Re – ^{187}Os isotope and highly siderophile element abundance systematics of shergottite meteorites. *Geochim. Cosmochim. Acta* **76**, 206–235.
- Brenan J. M., Bennett N. R. and Zajacz Z. (2016) Experimental results on fractionation of the highly siderophile elements (HSE) at variable pressures and temperatures during planetary and magmatic differentiation. *Rev. Mineral. Geochem.* **81**, 1–87.
- Breton T. and Quitté G. (2014) High-precision measurements of tungsten stable isotopes and application to earth sciences. *J. Anal. At. Spectrom.* **29**, 2284–2293.
- Breton T., Quitté G., Toplis M. J., Monnereau M., Birck J.-L., Göpel C. and Charles C. (2015) Tafassasset: evidence of early incipient differentiation on a metal-rich chondritic parent body. *Earth Planet. Sci. Lett.* **425**, 193–203.
- Burkhardt C., Kleine T., Dauphas N. and Wieler R. (2012) Nucleosynthetic tungsten isotope anomalies in acid leachates of the Murchison chondrite: implications for hafnium–tungsten chronometry. *Astrophys. J. Lett.* **753**, L6.
- Burkhardt C. and Schönbächler M. (2015) Intrinsic W nucleosynthetic isotope variations in carbonaceous chondrites: implications for W nucleosynthesis and nebular vs. parent body processing of presolar materials. *Geochim. Cosmochim. Acta* **165**, 361–375.
- Budde G., Kleine T., Kruijjer T. S., Burkhardt C. and Metzler K. (2016) Tungsten isotopic constraints on the age and origin of chondrules. *Proc. National Acad. Sci.* **113**, 2886–2891.
- Budde G., Kruijjer T. S. and Kleine T. (2018) Hf–W chronology of CR chondrites: implications for the timescales of chondrule formation and the distribution of ^{26}Al in the solar nebula. *Geochim. Cosmochim. Acta* **222**, 284–304.
- Cherniak D. J. and Van Orman J. A. (2014) Tungsten diffusion in olivine. *Geochim. Cosmochim. Acta* **129**, 1–12.
- Chou C.-L., Baedecker P. A. and Wasson J. T. (1973) Distribution of Ni, Ga, Ge and Ir between metal and silicate portions of H group chondrites. *Geochim. Cosmochim. Acta* **37**, 2159–2171.
- Cohen A. S. and Waters F. G. (1996) Separation of osmium from geological materials by solvent extraction for analysis by thermal ionisation mass spectrometry. *Anal. Chim. Acta* **332**, 269–275.
- Connolly H. C., Huss G. R. and Wasserburg G. J. (2001) On the formation of Fe–Ni metal in Renazzo-like carbonaceous chondrites. *Geochim. Cosmochim. Acta* **65**, 4567–4588.
- Cook D. L. and Schönbächler M. (2016) High-precision measurement of W isotopes in Fe–Ni alloy and the effects from the nuclear field shift. *J. Anal. At. Spectrom.* **31**, 1400–1405.
- Cottrell E., Walter M. J. and Walker D. (2009) Metal–silicate partitioning of tungsten at high pressure and temperature: implications for equilibrium core formation in Earth. *Earth Planet. Sci. Lett.* **281**, 275–287.
- Creaser R. A., Papanastassiou D. A. and Wasserburg G. J. (1991) Negative thermal ion mass spectrometry of osmium, rhenium and iridium. *Geochim. Cosmochim. Acta* **55**, 397–401.
- Fortenfant S. S., Günther D., Dingwell D. B. and Rubie D. C. (2003) Temperature dependence of Pt and Rh solubilities in a haplobasaltic melt. *Geochim. Cosmochim. Acta* **67**, 123–131.
- Ganguly J., Tirone M., Chakraborty S. and Domanik K. (2013) H chondrite parent asteroid: a multistage cooling, fragmentation and re-accretion history constrained by thermometric studies, diffusion kinetic modeling and geochronological data. *Geochim. Cosmochim. Acta* **105**, 206–220.
- Garçon M., Boyet M., Carlson R. W., Horan M. F., Auclair D. and Mock T. D. (2018) Factors influencing the precision and accuracy of Nd isotope measurements by thermal ionization mass spectrometry. *Chem. Geol.* **476**, 493–514.
- Göpel C., Manhès G. and Allegre C. J. (1994) U–Pb systematics of phosphates from equilibrated ordinary chondrites. *Earth Planet. Sci. Lett.* **121**, 153–171.

- Göpel C., Birck J. L. and Manhès G. (2009) U/Pb and Cr isotope study of the Tafassasset meteorite. *Meteorit. Planet. Sci.* **44**, A83.
- Graf T. and Marti K. (1995) Collisional history of H chondrites. *J. Geophys. Res.* **100**, 21247–21264.
- Harrison K. P. and Grimm R. E. (2010) Thermal constraints on the early history of the H-chondrite parent body reconsidered. *Geochim. Cosmochim. Acta* **74**, 5410–5423.
- Harper C. L. and Jacobsen S. B. (1996) Evidence for ^{182}Hf in the early Solar System and constraints on the timescale of terrestrial accretion and core formation. *Geochim. Cosmochim. Acta* **60**, 1131–1153.
- Hayden L. A. and Watson E. B. (2007) A diffusion mechanism for core–mantle interaction. *Nature* **450**, 709–711.
- Hellmann J. L., Kruijer T. S., Van Orman J. A., Metzler K. and Kleine T. (2018) Hf–W chronology of ordinary chondrites: timing of metal–silicate fractionation and implications for the thermal and impact history of asteroids. *Earth Planet. Sci. Lett.* (in preparation).
- Henke S., Gail H.-P., Trierloff M., Schwarz W. H. and Kleine T. (2012) Thermal history modeling of the H chondrite parent body. *Astron. Astrophys.* **545**, A135.
- Horan M. F., Walker R. J., Morgan J. W., Grossman J. N. and Rubin A. E. (2003) Highly siderophile elements in chondrites. *Chem. Geol.* **196**, 5–20.
- Horan M. F., Alexander C. M. O'D. and Walker R. J. (2009) Highly siderophile element evidence for early Solar System processes in components from ordinary chondrites. *Geochim. Cosmochim. Acta* **73**, 6984–6997.
- Humayun M. and Campbell A. J. (2002) The duration of ordinary chondrite metamorphism inferred from tungsten microdistribution in metal. *Earth Planet. Sci. Lett.* **198**, 225–243.
- Humayun M. (2012) Chondrule cooling rates inferred from diffusive profiles in metal lumps from the Acfer 097 CR2 chondrite. *Meteorit. Planet. Sci.* **47**, 1191–1208.
- Huss G. R., Rubin A. E. and Grossman J. N. (2006) Thermal metamorphism in chondrites. In *Meteorites and the Early Solar System II* (eds. D. S. Lauretta and H. Y. McSween). The University of Arizona Press, Tucson, pp. 567–586.
- Jost W. (1960) Diffusion in Solids, Liquids, Gases. Academic Press Inc.
- Kadlag Y. and Becker H. (2016) ^{187}Re – ^{187}Os systematics, highly siderophile and chalcogen element abundances in the components of unequilibrated L chondrites. *Geochim. Cosmochim. Acta* **172**, 225–246.
- Keil K. (2000) Thermal alteration of asteroids: Evidence from meteorites. *Planet. Space Sci.* **48**, 887–903.
- Kimura K., Lewis R. S. and Anders E. (1974) Distribution of gold and rhenium between nickel–iron and silicate melts: implications for the abundance of siderophile elements on the Earth and Moon. *Geochim. Cosmochim. Acta* **38**, 683–701.
- Kleine T., Mezger K., Münker C., Palme H. and Bischoff A. (2004) ^{182}Hf – ^{182}W isotope systematics of chondrites, eucrites, and Martian meteorites: chronology of core formation and early mantle differentiation in Vesta and Mars. *Geochim. Cosmochim. Acta* **68**, 2935–2946.
- Kleine T., Mezger K., Palme H., Scherer E. and Münker C. (2005) Early core formation in asteroids and late accretion of chondrite parent bodies: evidence from ^{182}Hf – ^{182}W in CAIs, metal-rich chondrites and iron meteorites. *Geochim. Cosmochim. Acta* **69**, 5805–5818.
- Kleine T., Touboul M., Halliday A., Zipfel J. and Palme H. (2007) Cosmochemical fractionation of Hf and W in the solar nebula: evidence from W isotopes in chondrites. *Lunar Planet. Sci. XXXVIII. Lunar Planet. Inst., Houston.* #2362 (abstr.).
- Kleine T., Touboul M., Van Orman J. A., Bourdon B., Maden C., Mezger K. and Halliday A. (2008) Hf–W thermochronometry: closure temperature and constraints on the accretion and cooling history of the H chondrite parent body. *Earth Planet. Sci. Lett.* **270**, 106–118.
- Kleine T., Hans U., Irving A. J. and Bourdon B. (2012) Chronology of the angrite parent body and implications for core formation in protoplanets. *Geochim. Cosmochim. Acta* **84**, 186–203.
- Kong P. and Ebihara M. (1996) Distribution of W and Mo in ordinary chondrites and implications for nebular and parent body thermal processes. *Earth Planet. Sci. Lett.* **137**, 83–93.
- Krot A. N., Meibom A., Weisberg M. K. and Keil K. (2002) The CR chondrite clan: Implications for early solar system processes. *Meteorit. Planet. Sci.* **37**, 1451–1490.
- Kruijer T. S., Sprung P., Kleine T., Leya I., Burkhardt C. and Wieler R. (2012) Hf–W chronometry of core formation in planetesimals inferred from weakly irradiated iron meteorites. *Geochim. Cosmochim. Acta* **99**, 287–304.
- Kruijer T. S., Fischer-Gödde M., Kleine T., Sprung P., Leya I. and Wieler R. (2013) Neutron capture on Pt isotopes in iron meteorites and the Hf–W chronology of core formation in planetesimals. *Earth Planet. Sci. Lett.* **361**, 162–172.
- Kruijer T. S., Touboul M., Fischer-Gödde M., Birmingham K. R., Walker R. J. and Kleine T. (2014a) Protracted core formation and rapid accretion of protoplanets. *Science* **344**, 1150–1154.
- Kruijer T. S., Kleine T., Fischer-Gödde M., Burkhardt C. and Wieler R. (2014b) Nucleosynthetic W isotope anomalies and the Hf–W chronometry of Ca–Al-rich inclusions. *Earth Planet. Sci. Lett.* **403**, 317–327.
- Kruijer T. S., Kleine T., Fischer-Gödde M. and Sprung P. (2015) Lunar tungsten isotopic evidence for the late veneer. *Nature* **520**, 534–537.
- Kruijer T. S., Burkhardt C., Budde G. and Kleine T. (2017) Age of Jupiter inferred from the distinct genetics and formation times of meteorites. *Proc. National Acad. Sci.* **114**, 6712–6716.
- Lee D. C. and Halliday A. N. (1995) Hafnium–tungsten chronometry and the timing of terrestrial core formation. *Nature* **378**, 771–774.
- Ludwig K. R. (2001) *Users Manual for Isoplot/Ex version 2.47. A geochronological toolkit for Microsoft Excel*. Berkeley Geochronology Center Special Publication, 55 pp.
- Markowski A., Leya I., Quitté G., Ammon K., Halliday A. N. and Wieler R. (2006a) Correlated helium-3 and tungsten isotopes in iron meteorites: quantitative cosmogenic corrections and planetesimal formation times. *Earth Planet. Sci. Lett.* **250**, 104–115.
- Markowski A., Quitté G., Halliday A. N. and Kleine T. (2006b) Tungsten isotopic compositions of iron meteorites: chronological constraints vs. cosmogenic effects. *Earth Planet. Sci. Lett.* **242**, 1–15.
- Monnereau M., Toplis M. J., Baratoux D. and Guignard J. (2013) Thermal history of the H-chondrite parent body: implications for metamorphic grade and accretionary time-scales. *Geochim. Cosmochim. Acta* **119**, 302–321.
- Mundl A., Walker R. J., Reimink J. R., Rudnick R. L. and Gaschnig R. M. (2018) Tungsten-182 in the upper continental crust: evidence from glacial diamictites. *Chem. Geol.* **494**, 144–152.
- Myers R. J. and Metzler D. E. (1950) The distribution of ferric iron between hydrochloric acid and isopropyl ether solutions. II. Polymerization of the iron in the ether phase, the effect of the acid concentration on the distribution, and two ether-phase region. *J. Am. Chem. Soc.* **72**, 3772–3776.
- Newsom H. E. (1990) Accretion and core formation in the Earth: evidence from siderophile elements. In *Origin of the Earth* (eds.

- H. E. Newsom and J. H. Jones). Oxford Univ. Press, New York, pp. 273–288.
- Norris T. L., Gancarz A. J., Rokop D. J. and Thomas K. W. (1983) Half-life of ^{26}Al . *J. Geophys. Res.* **88**, B331–B333.
- O'Neill H. S. C., Dingwell D. B., Borisov A., Spettel B. and Palme H. (1995) Experimental petrochemistry of some highly siderophile elements at high temperatures, and some implications for core formation and the mantle's early history. *Chem. Geol.* **120**, 255–273.
- Pellas R. and Storzer D. (1981) ^{244}Pu fission track thermometry and its application to stony meteorites. *Proc. R. Soc. Lond. A: Math. Phys. Eng. Sci.* **374**, 253–270.
- Qin L., Dauphas N., Horan M. F., Leya I. and Carlson R. W. (2015) Correlated cosmogenic W and Os isotopic variations in Carbo and implications for Hf–W chronology. *Geochim. Cosmochim. Acta* **153**, 91–104.
- Quitté G., Birk J.-L. and Allégre C. J. (2005) Stony-iron meteorites: history of the metal phase according to tungsten isotopes. *Geochim. Cosmochim. Acta* **69**, 1321–1332.
- Rambaldi E. R. (1976) Trace element of metals from L-group chondrites. *Earth Planet. Sci. Lett.* **31**, 224–238.
- Rehkämper M. and Halliday A. N. (1997) Development and application of new ion-exchange techniques for the separation of the platinum group and other siderophile elements from geological samples. *Talanta* **44**, 663–672.
- Righter K. and Shearer C. K. (2003) Magmatic fractionation of Hf and W: constraints on the timing of core formation and differentiation in the Moon and Mars. *Geochim. Cosmochim. Acta* **67**, 2497–2507.
- Rubin A. E. (1999) Formation of large metal nodules in ordinary chondrites. *J. Geophys. Res.* **104**, 30799–30804.
- Rubin A. E. (2000) Petrologic, geochemical and experimental constraints on models of chondrule formation. *Earth Sci. Rev.* **50**, 3–27.
- Rubin A. E., Ulff-Møller F., Wasson J. T. and Carlson W. D. (2001) The Portales Valley meteorite breccia: evidence for impact-induced melting and metamorphism of an ordinary chondrite. *Geochim. Cosmochim. Acta* **65**, 323–342.
- Ruzicka A., Hugo R. and Hutson M. (2015) Deformation and thermal histories of ordinary chondrites: evidence for postdeformation annealing and syn-metamorphic shock. *Geochim. Cosmochim. Acta* **163**, 219–233.
- Scott E. R., Krot T. V., Goldstein J. I. and Wakita S. (2014) Thermal and impact history of the H chondrite parent asteroid during metamorphism: constraints from metallic Fe–Ni. *Geochim. Cosmochim. Acta* **136**, 13–37.
- Shirey S. B. and Walker R. J. (1995) Carius tube digestion for low blank rhenium-osmium analysis. *Anal. Chem.* **67**, 2136–2141.
- Slater-Reynolds V. and McSween H. Y. (2005) Peak metamorphic temperatures in type 6 ordinary chondrites: an evaluation of pyroxene and plagioclase geothermometry. *Meteorit. Planet. Sci.* **40**, 745–754.
- Smoliar M. I., Walker R. J. and Morgan J. W. (1996) Re–Os ages of group IIA, IIIA, IVA, and IVB iron meteorites. *Science* **271**, 1099–1102.
- Taylor G. J., Maggiore P., Scott E. R., Rubin A. E. and Keil K. (1987) Original structures, and fragmentation and reassembly histories of asteroids: evidence from meteorites. *Icarus* **69**, 1–13.
- Touboul M., Kleine T., Bourdon B., Palme H. and Wieler R. (2007) Late formation and prolonged differentiation of the Moon inferred from W isotopes in lunar metals. *Nature* **450**, 1206–1209.
- Touboul M., Kleine T., Bourdon B., Van Orman J. A., Maden C. and Zipfel J. (2009) Hf–W thermochronometry: II. Accretion and thermal history of the acapulcoite-lodranite parent body. *Earth Planet. Sci. Lett.* **284**, 168–178.
- Touboul M. and Walker R. J. (2012) High precision measurement of tungsten isotopes by thermal ionization mass spectrometry. *Int. J. Mass Spectrom.* **309**, 109–117.
- Trieloff M., Jessberger E. K., Herrwerth I., Hopp J., Fiéni C., Ghéllis M., Bourrot-Denise M. and Pellas P. (2003) Structure and thermal history of the H-chondrite parent asteroid revealed by thermochronometry. *Nature* **422**, 502–506.
- Van Orman J. A., Grove T. L. and Shimizu N. (2001) Rare earth element diffusion in diopside: influence of temperature, pressure, and ionic radius, and an elastic model for diffusion in silicates. *Contrib. Mineral. Petrol.* **141**, 687–703.
- Vockenhuber C., Oberli F., Bichler M., Ahmad I., Quitté G., Meier M., Halliday A. N., Lee D. C., Kutschera W., Steier P., Gehrke R. J. and Helmer R. G. (2004) New half-life measurement of ^{182}Hf : improved chronometer for the early solar system. *Phys. Rev. Lett.* **93**, 172501.
- Wade J. and Wood B. J. (2005) Core formation and the oxidation state of the Earth. *Earth Planet. Sci. Lett.* **236**, 78–95.
- Walker R. J. (2012) Evidence for homogenous distribution of osmium in the protosolar nebula. *Earth Planet. Sci. Lett.* **351–352**, 36–44.
- Walker R. J., Horan M. F., Morgan J. W., Becker H., Grossman J. N. and Rubin A. (2002) Comparative ^{187}Re – ^{187}Os systematics of chondrites: implications regarding early solar system processes. *Geochim. Cosmochim. Acta* **66**, 4187–4201.
- Walker R. J., Yin Q.-Z. and Heck P. R. (2018) Rapid effects of terrestrial alteration on highly siderophile elements in the Sutter's Mill meteorite. *Meteorit. Planet. Sci.* **53**, 1500–1506.
- Walter M. J., Newsom H. E., Ertel W. and Holzheid A. (2000) Siderophile elements in the Earth and Moon. Metal/Silicate partitioning and implication for core formation. In *Origin of the Earth and Moon* (eds. R. M. Canup and K. Righter). University of Arizona Press, Tucson, pp. 265–289.
- Wasson J. T. and Rubin A. E. (2010) Metal in CR chondrites. *Geochim. Cosmochim. Acta* **74**, 2212–2230.
- Weisberg M. K., Prinz M., Clayton R. N. and Mayeda T. K. (1993) The CR (Renazzo-type) carbonaceous chondrite group and its implications. *Geochim. Cosmochim. Acta* **57**, 1567–1586.
- Weisberg M. K., Prinz M., Clayton R. N., Mayeda T. K., Grady M. M. and Pillinger C. T. (1995) The CR chondrite clan. *Proc. NIPR Symp. Antarct. Meteorit.* **8**, 11–32.
- Weisberg M. K., McCoy T. J. and Krot A. N. (2006) Systematics and evaluation of meteorite classification. In *Meteorites and the Early Solar System II* (eds. D. S. Lauretta and H. Y. McSween). The University of Arizona Press, Tucson, pp. 19–52.
- Willbold M., Elliott T. and Moorbath S. (2011) The tungsten isotopic composition of the Earth's mantle before the terminal bombardment. *Nature* **477**, 195–198.
- Wittig N., Humayun M., Brandon A. D., Huang S. and Leya I. (2013) Coupled W–Os–Pt isotope systematics in IVB iron meteorites: in situ neutron dosimetry for W isotope chronology. *Earth Planet. Sci. Lett.* **361**, 152–161.
- Worsham E. A., Bermingham K. R. and Walker R. J. (2017) Characterizing cosmochemical materials with genetic affinities to the Earth: genetic and chronological diversity within the IAB iron meteorite complex. *Earth Planet. Sci. Lett.* **467**, 157–166.
- Yokoyama T., Walker D. and Walker R. J. (2009) Low osmium solubility in silicate at high pressures and temperatures. *Earth Planet. Sci. Lett.* **279**, 165–173.
- Zanda B., Bourrot-Denise M., Perron C. and Hewins R. H. (1994) Origin and metamorphic redistribution of silicon, chromium, and phosphorus in the metal of chondrites. *Science* **265**, 1846–1849.